Università degli Studi di Napoli Federico II

Scuola Politecnica e delle Scienze di Base

Dipartimento di Ingegneria Industriale

Corso di Laurea in Ingegneria Aerospaziale
Classe delle Lauree in Ingegneria Industriale (L-9)

Elaborato di Laurea in Meccanica del Volo

Effects of the distributed propulsion on the stability and control characteristics of a 19-pax aircraft model

Relatore
Prof. Danilo Ciliberti

Candidato
Giulia Marchetta
N35/3949

Anno Accademico 2023–2024

A Lello, ai miei nonni e a tutti coloro che hanno sempre creduto in me, questo traguardo è anche vostro.

Abstract

The aim of this work is to analyse stability and control effects of the distributed propulsion on a 19-pax aircraft model. The objective is reached through OpenVSP, an open-source tool developed by NASA, and VSPAERO. The former is a parametric aircraft geometry software which allows to create a 3D model of the aircraft, giving reliable engineering results after a careful data set up. The latter is a vortex lattice solver, developed by NASA's research center, that uses OpenVSP geometries to evaluate aircraft performances in different flow configurations. Particularly, through OpenVSP, it was possible to use actuator disks in order to simplify the modelisation of propellers. In this way comparisons of propellers-on and propellers-off results are accomplished and, accordingly, benefits of distributed electric propulsion are evaluated.

Sommario

Lo scopo di questo lavoro è analizzare gli effetti di stabilità e controllo della propulsione distribuita su un modello di aereo da 19 posti. L'obiettivo è raggiunto tramite l'utilizzo di OpenVSP, cioè uno strumento open-source sviluppato dalla NASA, e VSPAERO. Il primo è un software di geometria parametrica di un velivolo che permette di creare un modello 3D dell'aereo, fornendo risultati ingegneristici affidabili dopo un'attenta impostazione dei dati. Il secondo è un solutore di vortici a reticolo, sviluppato dal centro di ricerca della NASA, che utilizza le geometrie di OpenVSP per valutare le prestazioni del velivolo in diverse configurazioni di flusso. In particolare, attraverso OpenVSP è stato possibile utilizzare dischi attuatori per semplificare la modellazione delle eliche. In questo modo è possibile confrontare i risultati ottenuti con le eliche e quelli ottenuti senza eliche e, di conseguenza, valutare i vantaggi della propulsione elettrica distribuita.

Contents

List of Figures

Chapter 1

Introduction

1.1 Objective

The purpose of this thesis is to reveal the effects of the distributed propulsion on the stability and control characteristics of a 19-pax aircraft model that would be tested in the wind tunnel. First, the aircraft was modelled with the geometric modeller OpenVSP with 10 propellers located ahead of the wings as actuator disks. Then analysis was performed with the vortex latex solver VSPAERO, with 8 disks simulating propellers driven by electric motors and 2 disks simulating larger propellers driven by thermal engines. Afterward, the results were collected, organised, and plotted on spreadsheet, describing the aerodynamic forces and moments of the complete aircraft. Therefore, the effects of flaps and control surfaces on the longitudinal and latero-directional stability and control characteristics were evaluated with and without propellers.

1.2 Layout of the work

Chapter 2: This chapter is about theoretical principles and methods which this thesis project is based on.
Chapter 3: This chapter highlights the aircraft geometry and the tools used for modeling and analysing it.
Chapter 4: This section concerns the process of aerodynamic coefficients analysis and the effects observed, represented through graphs and comparison table.
Chapter 5: This chapter points out aerodynamic derivatives that enable to understand curves slope so as stability and control consideration are done.
Chapter 6: Conclusion chapter.

Chapter 2

Theoretical overview

2.1 DEP principle

Distributed Electric Propulsion (DEP) principle is to use propellers which primary use is to enhance high-lift instead to be optimised for thrust. The flow over a lifting surface would be accelerated in low velocity conditions, hence more lift would be produced per given airspeed, angle of attack, and planform area, enabling a beneficial aero-propulsive coupling.

The application of DEP could offer gains with respect to traditional internal combustion engines, such as the flexible architectures and the multiple combinations of wing and propeller parameters used to build the most efficient aircraft for having best performance compared to the conventional design. Moreover new studies [2]have shown that the use of DEP offers alternatives to increase control capability while a high bypass ratio systems lead to substantial enhancing of performance.

DEP aircraft concepts have been designed with several functional capabilities, including conventional take-off and landing, short take-off and landing, as well as electric vertical take-off and landing.

DEP allows aircraft to increase their efficiency for the engine as well as lift-to-drag ratio. In particular, one could consider the efficiency gain with the ratio of the energy consumption of an aircraft retrofitted with DEP to the energy consumption of an unmodified aircraft. The main objective is to keep low-speed performance, without sacrificing cruise performance.

This goal could be achieved since distributed propellers allow a reduction of wing area, so that the aircraft would be lighter and more compact, and a potential reduction of cruise drag, especially with propellers close to the wing tip. Moreover, the distributed thrust over a large number of propellers should enable slower and hence quieter take-off and landing operations [1].

Furthermore new high-lift propellers designs were introduced. These have a different shape compared to the traditional one, with an increased chord and twist angle close to the blade root and decreased values in the middle, with a view to augment lift maintaining a uniform axial velocity profile in the propeller slipstream. For the same reason, the twist angle is increased at the tip of the blade. It is clear observing Figure 2.1 how axial velocity changes in high-lift propeller blades versus the traditional ones (i.e., Minimum Induced Loss — MIL — designs).

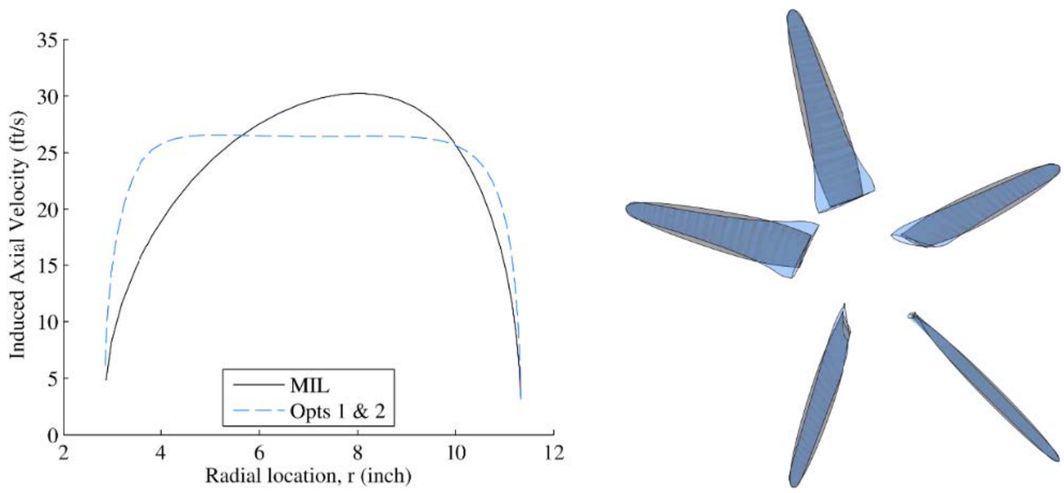

Figure 2.1: Comparison between high-lift propellers design (dashed curve) and conventional propellers design (solid curve) [1].

DEP propellers could be implemented in different ways, for example in Figure 2.2 it can be observed, along the leading edge of the wing, high-lift propellers used to enhance low-speed flow increasing dynamic pressure by blowing on the wing and at the wingtips primary propulsive power propellers, that decrease the induced drag boosting the lift-to-drag ratio.

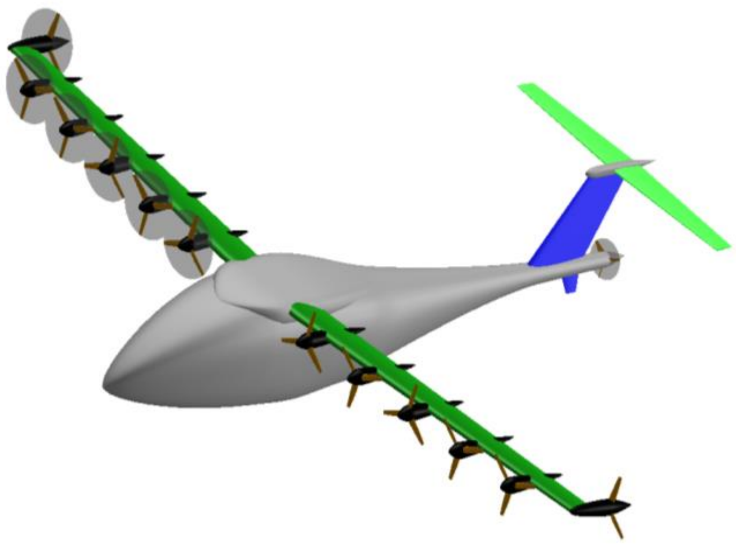

Figure 2.2: DEP Different Implementation

It is possible to find a drawback in high-lift distributed propellers configurations because actually these have a small range without a substantial energy stored weight penalty, and another disadvantage is structural robustness.

Before integrating DEP aircraft into large-scale vehicle systems, it is necessary to develop electrical system technologies which are presently employed in small-scale unmanned and passenger air vehicles. Ongoing DEP research aims to enhance the maximum power capabilities and electrical machines power beyond current standards [2].

2.2 Actuator Disk Theory

Actuator disk theory, also know as momentum theory is a fundamental concept in the field of fluid mechanics and is often used in the design of pumps, fans, and turbines or, as in the case of this work, propellers. Generally this theory focuses on the dynamic of the the interaction between the rotating disk and the fluid. The idea is to apply conservation laws of fluid mechanics to the rotor and flows. Particularly behind this theory there are some considerations to evaluate [3]:

- the propeller is modeled as an actuator disk;
- the actuator disk is often idealized as a thin, flat disk, with a projected frontal area A. It may not accurately represent the effective behavior of the rotor;
- the actuator disk theory assumes that the flow of the fluid is incompressible and inviscid, meaning that there is no frictional resistance between fluid layers;
- the propeller is characterized by a pressure jump that accelerate the air through the disk;
- the analysis often assumes steady-state flow conditions, where the flow properties do not change, simplifying mathematical formulation;
- static pressures far from disk are assumed equal to atmospheric pressure;
- the actuator disk provides a smooth change on flow velocity, accelerating it downstream.

The main objectives of the actuator disk theory are:

1. predict the amount of thrust generated by the propeller;
2. optimise the propeller design, so that aircraft performance could be enhanced;
3. analyse the aerodynamic loads distribution along the length of propellers.

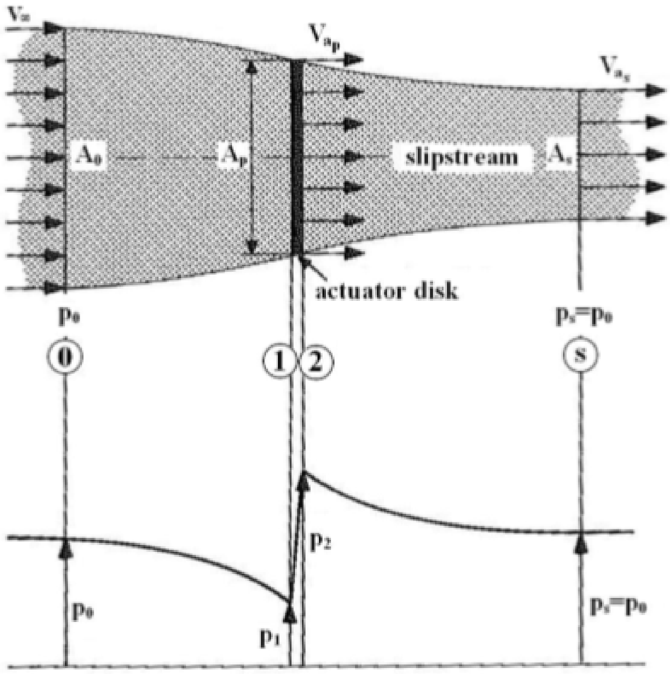

Figure 2.3: Velocity and static pressure distribution due to momentum theory.

Propeller thrust is:

$$T = \rho V_{as} A_s (V_{as} - V_\infty) \tag{2.1}$$

where V_{as} is the downstream velocity, where pressure is assumed at ambient value, and A_s is the cross sectional area of the slipstream, which is variable along the slipstream. Meanwhile thrust can also be written as:

$$T = A_p(p_2 - p_1) = A_p \Delta p \tag{2.2}$$

where A_p is the propeller disk area. With the application of the Bernoulli's theorem it is possible to derive the following upstream equation:

$$p_0 + \frac{1}{2}\rho V_\infty^2 = p_1 + \frac{1}{2}\rho V_{ap}^2 \tag{2.3}$$

while for the downstream:

$$p_2 + \frac{1}{2}\rho V_{ap}^2 = p_0 + \frac{1}{2}\rho V_{as}^2 \tag{2.4}$$

The subtraction of the last two equations gives as a result the pressure jump:

$$\Delta p = \frac{1}{2}(V_{as}^2 - V_\infty^2) \tag{2.5}$$

Replacing the last one in (2.2) yields to:

$$T = \frac{1}{2}\rho A_p (V_{ap}^2 - V_\infty^2)\,. \tag{2.6}$$

Then considering the continuity equation:

$$V_{ap} A_p = V_{as} A_s \tag{2.7}$$

that can be combined with equations (2.1), (2.6), and (2.7), leading to:

$$V_{ap} = \frac{1}{2}(V_\infty + V_{as})\,. \tag{2.8}$$

This equation shows that the arithmetic means between V_∞, i.e. the free-stream velocity, and V_{as}, i.e. the axial slipstream velocity. The propeller power is equal to the product of the thrust T and the the actuator disk velocity V_{ap}:

$$P = \frac{1}{2}\rho A_p V_{ap} (V_{as}^2 - V_\infty^2) \tag{2.9}$$

whereas propulsive efficiency is $\eta = TV_\infty/P$, and substituting equations (2.6) and (2.9) we obtain:

$$\eta = \frac{2V_\infty}{V_{as} + V_\infty}\,. \tag{2.10}$$

Ultimately by replacing equation (2.8) in (2.10) we have:

$$\eta = \frac{V_\infty}{V_{ap}}. \tag{2.11}$$

In conclusion, the application of the actuator disk theory to propellers plays a crucial role in the design and analysis of aircraft propulsion systems. Understanding the aerodynamic principles behind propeller enables the optimization of propeller designs, leading to enhanced efficiency and performance.

2.3 Vortex Lattice Method

The vortex lattice method, (VLM), is a numerical method used in computational fluid dynamics, which models an aircraft surface, or part of it, into a finite number of vortexes to calculate lift curve, induced drag, and force distribution at the early stages of the design.

This method is carried out on these assumptions:

- the flow field is incompressible, inviscid, and irrotational;
- the lifting surfaces are considered thin, neglecting the effects of thickness on aerodynamic forces;
- small angle approximation is employed, i.e., both the angle of attack and the angle of side-slip are assumed to be small.

The vortex lattice method is founded on the theory of ideal flow, also known as potential flow. Essentially the vortex lattice method divides the lifting surface into a grid of small panels or cells, thus facilitating the analysis of their performance characteristics. Each panel is assumed to generate a local vortex, which have to satisfy certain boundary conditions, typically based on the Kutta condition [4].Vortex lattice methods are based on solutions to Laplace's Equation. Starting with irrotational flow we have:

$$\nabla \times V = 0 \tag{2.12}$$

and considering a potential Φ we obtain:

$$\nabla \times (\nabla\Phi) = 0\,. \tag{2.13}$$

The combination of (2.12) and (2.13) equations leads to:

$$V = \nabla\Phi\,. \tag{2.14}$$

The equation (2.14) represents the irrotational and incompressible flow. Since continuity equation is valid, is it possible to consider the following equation:

$$\nabla \cdot V = 0\,. \tag{2.15}$$

By the union of equations (2.14) and (2.15) we have:

$$\nabla \cdot (\nabla\Phi) = 0 \tag{2.16}$$

and likewise:

$$\nabla^2\Phi = 0\,. \tag{2.17}$$

Equation (2.17) is known as Laplace's Equation. Because of its linearity, any irrotational and incompressible flow can be described as the combination of aerodynamic singularities.

The problem can be easily solved applying some boundary conditions to Laplace's Equation:

1. the airfoil has to be symmetrical;

2. neglecting camber effect;

3. including the angle of attack effect on a flat surface.

Once stated Γ as the circulation vortex, r as the the perpendicular distance between the point and the vortex line, in two-dimensional field the induced velocity at a point, for a vortex line of infinite length, is:

$$V_\theta = \frac{\Gamma}{2\pi r}\,. \tag{2.18}$$

The circulation has positive sign in the clockwise direction, as its vorticity. In a three-dimensional space, it can be shown that the velocity induced at a point P from a point Q of a vortex element of length dl and strength Γ is

$$\mathrm{d}V_{\mathrm{P}} = \frac{\Gamma}{4\pi} \cdot \frac{\mathrm{d}l \times r_{\mathrm{PQ}}}{|r_{\mathrm{PQ}}|^3} \tag{2.19}$$

where r_{PQ} is the distance between the aforementioned points. Equation (2.19) is also known as Biot-Savart law [4]. The idea of the vortex in a point through a vortex filament is shown in Figure 2.4.

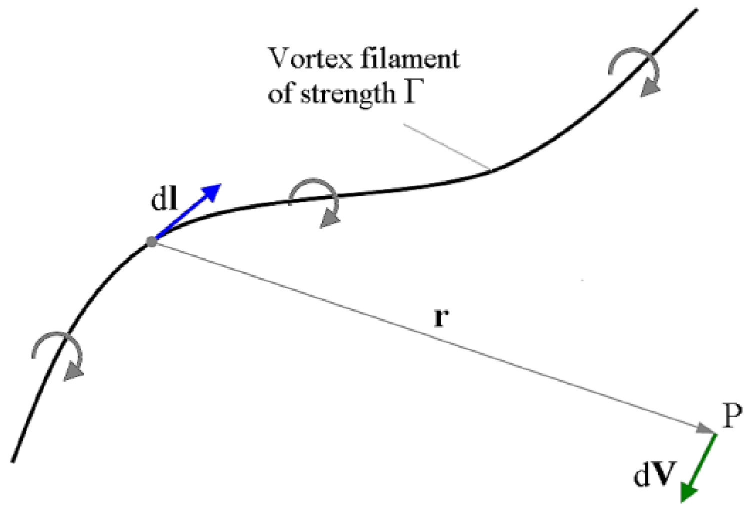

Figure 2.4: Velocity (dV) induced at a point P by an element of vortex filament (dl) of strength Γ.

At this point, Equation (2.19) could be integrated over the length of the vortex filament to derive the induced velocity at point P:

$$V_{\mathrm{P}} = \frac{\Gamma}{4\pi} \int \frac{\mathrm{d}l \times r_{\mathrm{PQ}}}{|r_{\mathrm{PQ}}|^3} . \tag{2.20}$$

As stated by the Kutta-Joukowski theorem, lift is generated by a

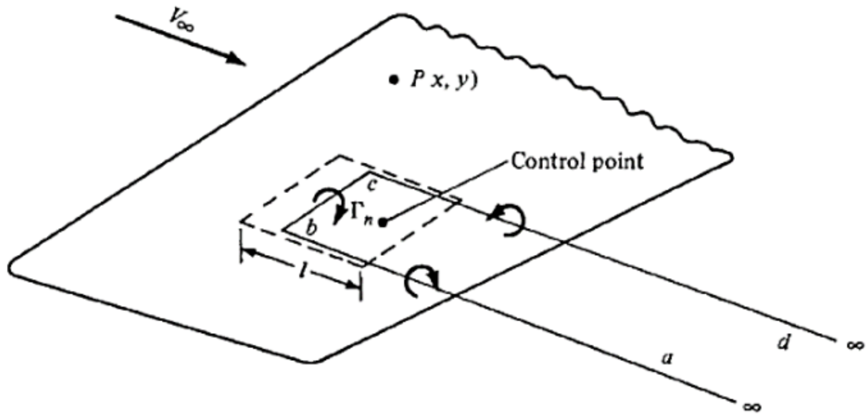

Figure 2.5: Horseshoe vortex scheme.

vortex with a circulation Γ, in stream velocity V_∞:

$$L = \rho_\infty V_\infty \Gamma \,. \tag{2.21}$$

Through VLM it is possible to simplify vortex as shown in Figure 2.5, where there are four vortex filaments whose velocity is represented by:

$$V = V_{bc} + V_{b\infty} + V_{c\infty} \tag{2.22}$$

where bc and ad vortex segments are finite, the other two are infinite and parallel to the direction of the free-stream velocity. This one is extracted by Biot-Savart law, considering initial boundary conditions.

One of the main problems related to VLM lies in its inaccurate results near the wing's leading and trailing edges, where thickness has a crucial role. While the method struggles to calculate actual local pressure distribution, it generally predicts total and local forces to an acceptable level. The finite set of horseshoe vortices stands for the continuous vorticity distribution along the wing surface.

In OpenVSP solver, vortex rings are employed, instead of the traditional VLM, with only trailing vortices extended to infinity.

This discretization of the wing and the ring elements is shown in Figure 2.6.

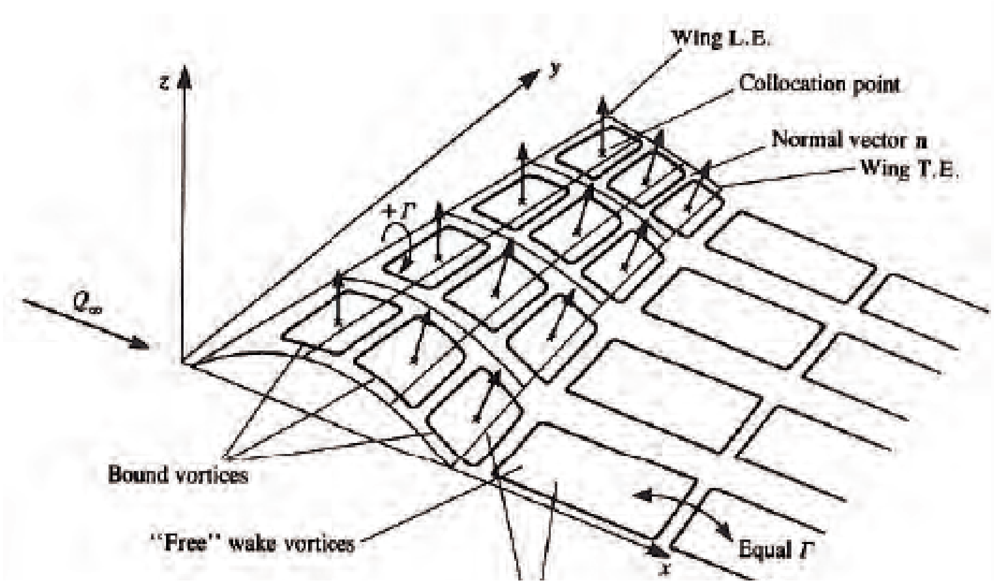

Figure 2.6: Ring vortex configuration.

Chapter 3

Modeling and Analysis Software

3.1 OpenVSP

OpenVSP stands for Open Vehicle Sketchpad. It was originated from earlier developments by J.R. Gloudemans and others for NASA in the early 1990s. In January 2012, it was released as an open-source project under the NOSA 1.3 license, with its initial open-source version being 2.0.0 [7].

OpenVSP is a software tool primarily utilised for parametric aircraft geometry design. It allows users to realise three-dimensional models of aircraft using several engineering parameters.

Through this software is possible to create an entire aircraft design starting with single components: first the wing, then the tail plane, the fuselage and after all the propellers, and then assembling all together.

The geometry panel opens, when the user selects a component. For each component it is important to set the Spanwise and Chordwise, respectively, U parameter and W parameter in Figure 3.1. These parameters allow the user to have more accurate analysis results.

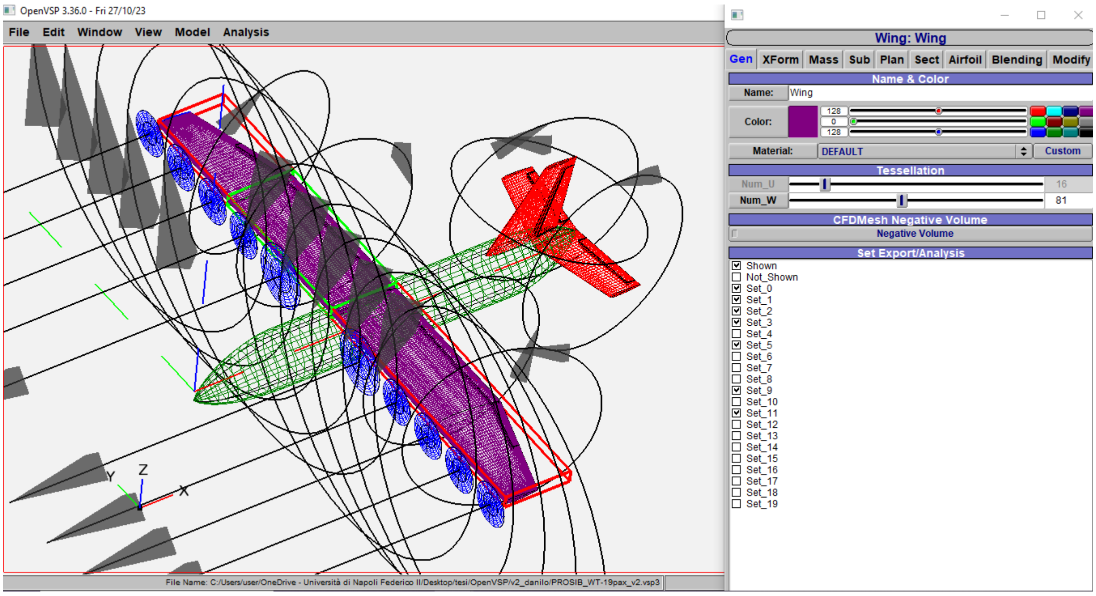

Figure 3.1: U and W setting in Geometry Wing Panel.

3.2 VSPAERO

VSPAERO is an open-source software developed by NASA, that is closely integrated with OpenVSP. Having OpenVSP geometries as models, VSPAERO employs VLM or Panel Method to carry on with aircraft analysis, set upping aircraft data as in Figure 3.2. This tool allows also the modelling of propellers as rotating blades or actuator disks.

The organization of control surface is simplified with a specific section named Control Grouping, which helps user make file configuration easier. Following directions on that page, as shown in Figure 3.3, a control surface can be assigned to multiple groups of components.

DegenGeom output files from OpenVSP are mainly analysed from VSPAERO that returns several files to the OpenVSP folder, containing important information to clarify the analyses as:

- LOD file contains input and span load information information, such as local lift, drag, and side force representation;
- HISTORY file has integrated moments and forces for each

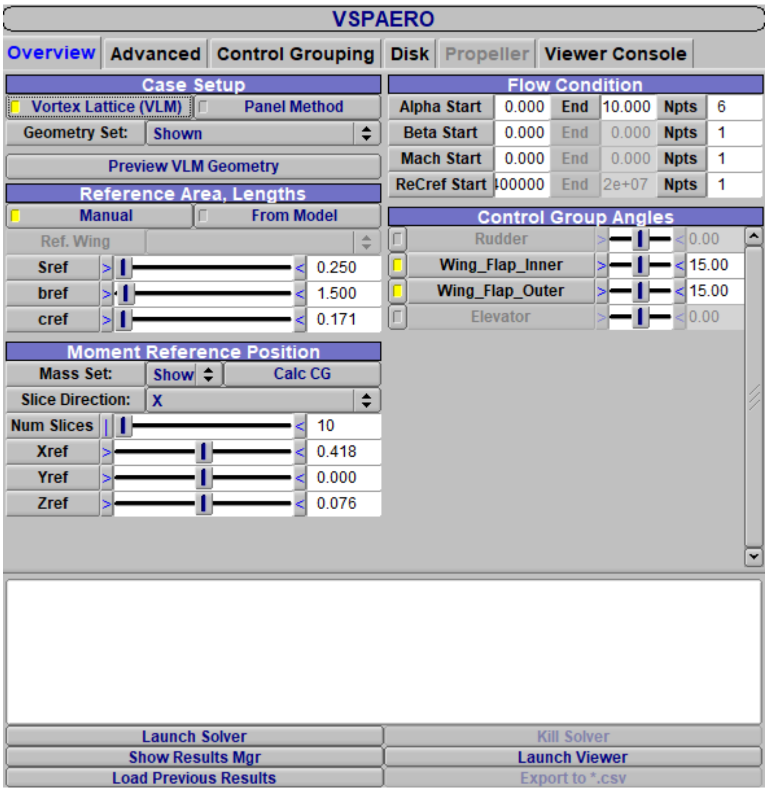

Figure 3.2: VSPAERO overview tab.

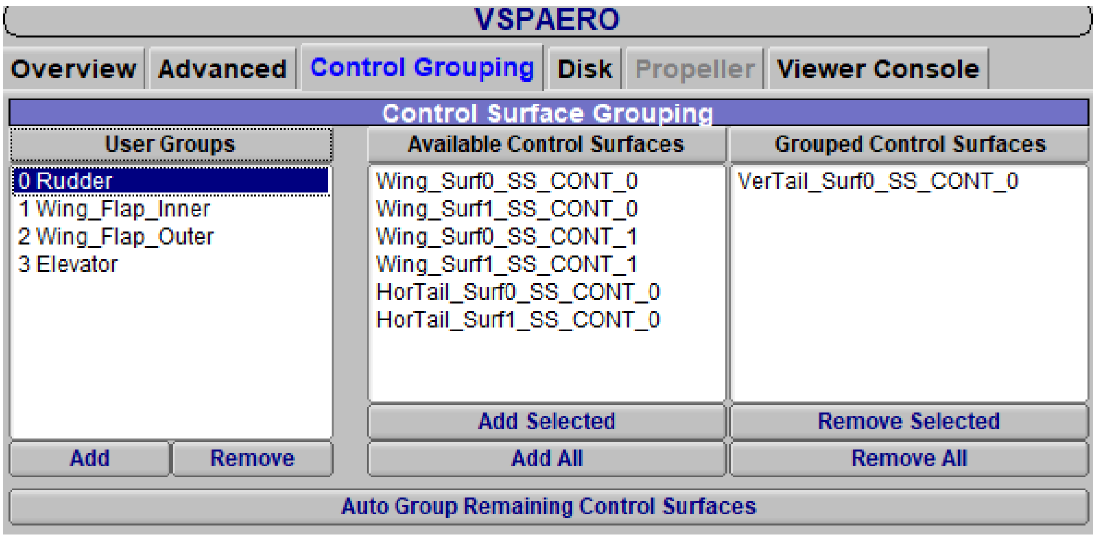

Figure 3.3: Control Surface Grouping overview section.

iteration, as computed by VSPAERO;

- POLAR file where forces and moment coefficient are shown within a table as input data changes.

3.3 Geometric Model

Aircraft geometric model is provided through OpenVSP and the earlier configuration in shown below in Figure 3.4 [5].

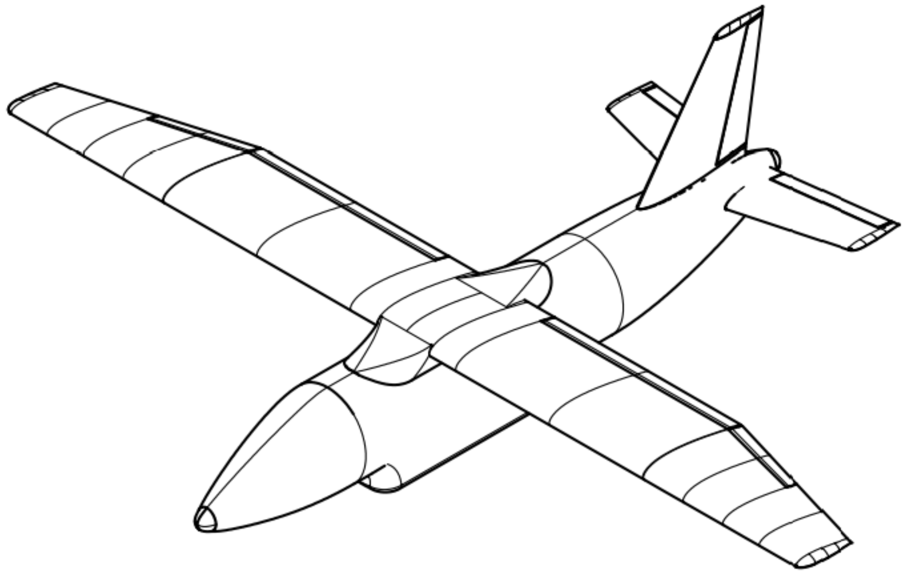

Figure 3.4: PROSIB 19-Pax aircraft model.

Ten propellers were added to the aircraft model, as in Figure 3.5. There are two propeller models:

- THERM propellers, closest to the fuselage, simulating the thrust provided by the thermal engines;
- DEP propellers, smaller and distributed over the rest of the wing, simulating thrust from electric motors.

Propellers have different characteristics shown in Tables 3.6 and 3.7.

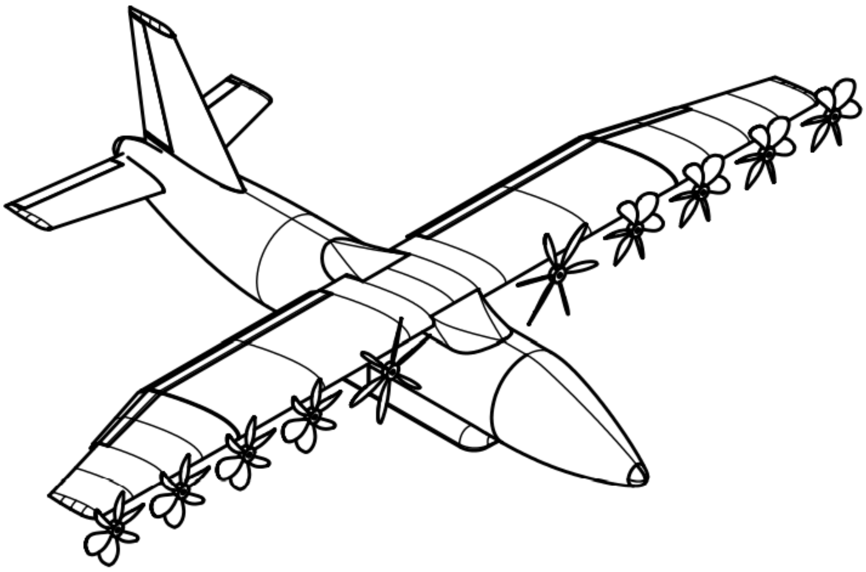

Figure 3.5: Aircraft model with propellers.

DATA	VALUE	MEASURE UNIT
Number of blades	6	/
Disk Radius	0.0845	m
Hub Radius	0.01	m
Design Speed	20	m/s
RPM	8000	RPM
Thrust	3.5	Newton
Altitude	0	km
Design Lift Coefficien	0.7	/
CT	0.158	/
CP	0.328	/
J	1.55	/

Figure 3.6: THERM propeller features.

DATA	VALUE	MEASURE UNIT
Number of blades	6	/
Disk Radius	0.0585	m
Hub Radius	0.01	m
Design Speed	20	m/s
RPM	10000	RPM
Thrust	4	Newton
Altitude	0	km
Design Lift Coefficien	0.7	/
CT	0.609	/
CP	1.383	/
J	1.03	/

Figure 3.7: DEP propeller features.

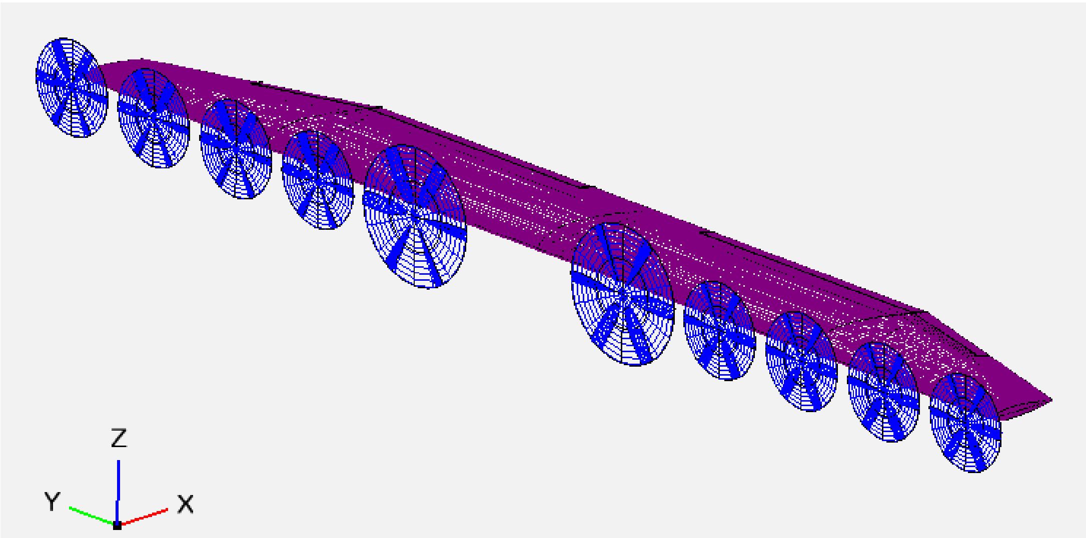

Figure 3.8: Blades implementation on wing.

It is possible to implement propellers in OpenVSP as actuator disks to simplify the studies, ignoring the blades' geometry. After setting up all the data in the software it is possible to create disks by selecting *Propeller* and choosing the option *Disk*, then setting the diameter and the number of blades, although the latter is not considered in the design. In Figure 3.8 it is shown how actuator disks are implemented on wings.

To continue with the analysis in VSPAERO, it is necessary to set the input data (Table 3.1).

INPUT DATA		
DATA	VALUE	M.U.
S_{ref}	0.250	m^2
b_{ref}	1500	m
c_{ref}	0.171	m
X_{ref}	0.418	m
Y_{ref}	0.000	m
Z_{ref}	0.076	m
AoA (start)	0.0	deg
AoA (end)	10.0	deg
Beta	0.0	deg
ρ_∞	1.225	kg/m^3
V_∞	20.0	m/s

Table 3.1: Table of VSPAERO input data.

Then by selecting *Disk*, we enter propeller data shown on Tables 3.6 and 3.7, setting them up as in shown in Figure 3.9.

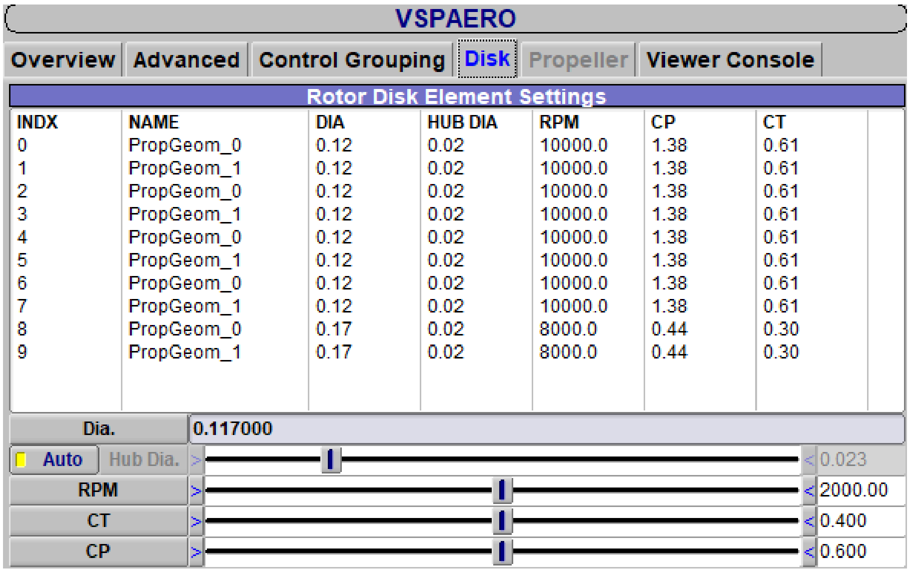

Figure 3.9: Actuator disk settings.

Chapter 4

Analyses and Results

4.1 Numerical setup

Analysis begins by adjusting the values in the Sect panel of the wing by setting in the *Wing Section 1* NumU=72, Rt.Cluster=1.00 and TipCluster=1.00, while in the *Wing Section 2* NumU=48, Rt.Cluster=1.00 and TipCluster=0.20, as shown in Figures 4.1 and 4.2.

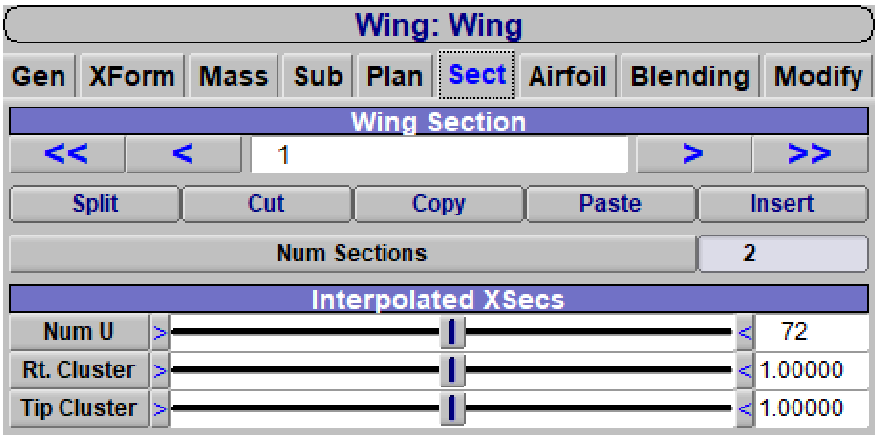

Figure 4.1: Wing Section 1.

VSPAERO also allows to analyse only specific parts of the aircraft from am entire geometry, organising such parts in sets. In this work, the selection of *Set 2* provided the analysis of the entire aircraft.

In addition, to make VSPAERO calculations more accurate and

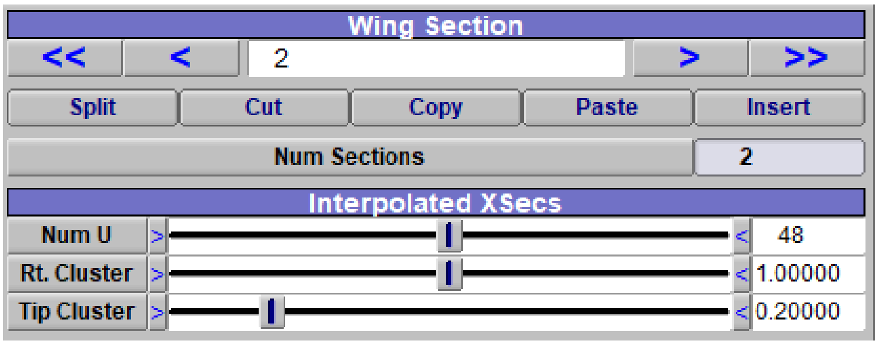

Figure 4.2: Wing Section 2.

faster, *2nd order Karman-Tsien Mach Correction* and *Matrix* as Preconditioner are selected in *Advanced* window, as in Figure 4.3.

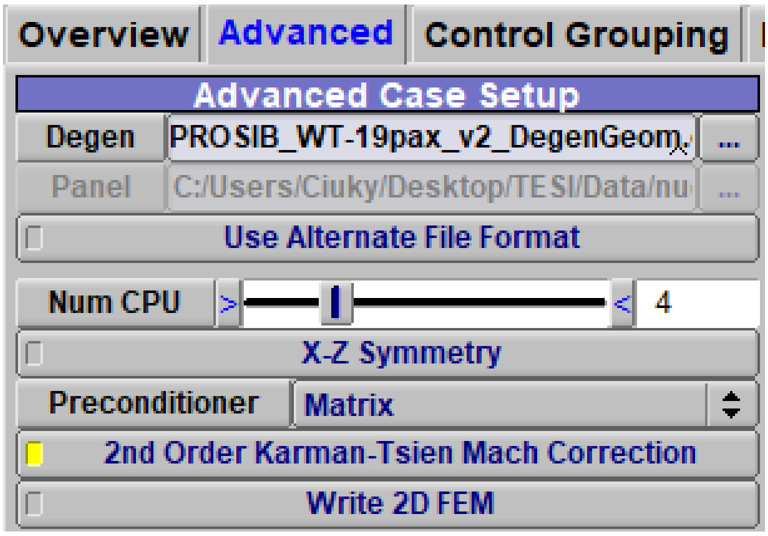

Figure 4.3: VSPAERO Advanced Case Setup.

4.2 Effects of DEP with angle of attack

In Figures 4.4, 4.5, 4.6, and 4.7, aerodynamic coefficient curves, comparing results with and without propeller, are plotted.

In these results, it can be seen that the C_{My} curve shifts upwards as shown in Figure 4.5. The trend of this curve is unusual, because as the C_L increases, the C_{My} should be more negative, but this set

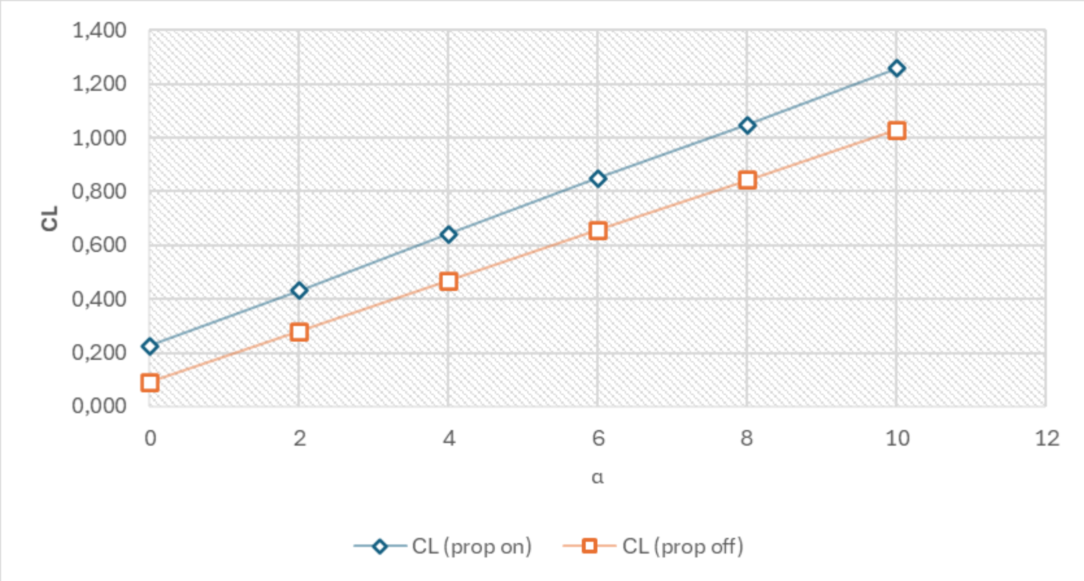

Figure 4.4: C_L vs. α comparison curves.

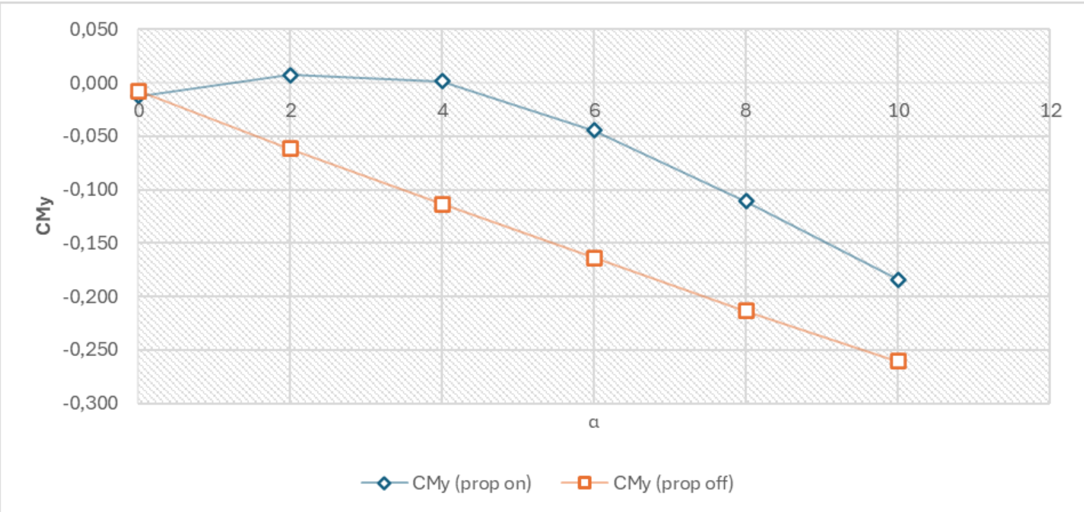

Figure 4.5: C_{My} vs. α comparison curves.

of propellers is causing this induction that makes the C_{My} a little more positive.

Observe that there is an aberration in drag coefficient C_D, since the prop-on values are negative. The source of this unrealistic result is the negative drag distribution over the wing span due to the flow induced by the propeller, as shown in Figures 4.8 and 4.9 for $\alpha = 4°$.

To further investigate the issue, another test was performed

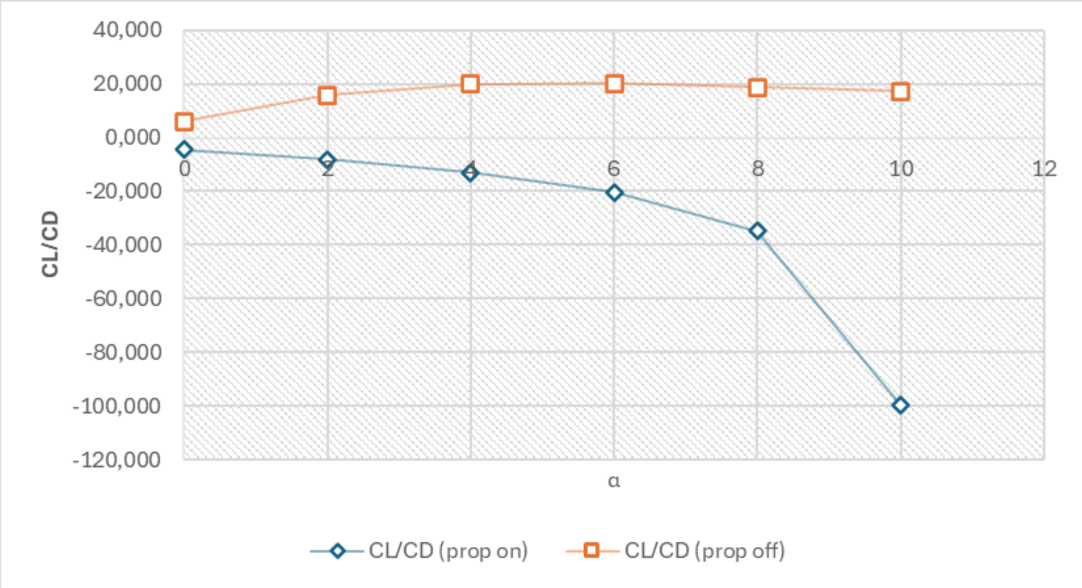

Figure 4.6: C_L/C_D vs. α comparison curves.

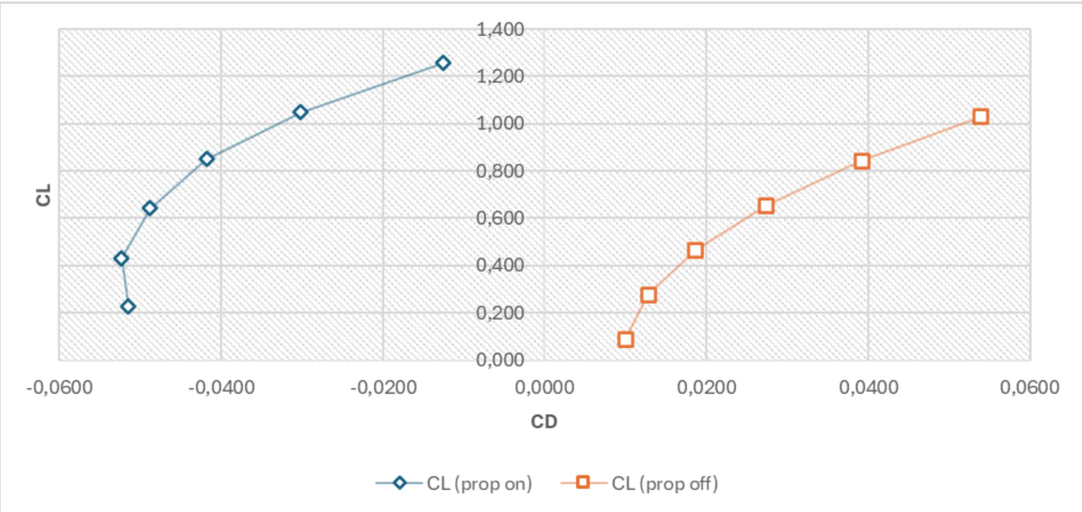

Figure 4.7: C_L vs. C_D comparison curves.

on the NASA X-57 aircraft model, which was downloaded from the OpenVSP hangar [6]. These analysis were done firstly with a velocity of 28 m/s, where in C_L vs. C_{Di} polar (the green one in Figure 4.10) there is a a slight part of the curve at which values of the coefficient drag are negative, while aerodynamic efficiency increases.

Another analysis was performed with same initial conditions and

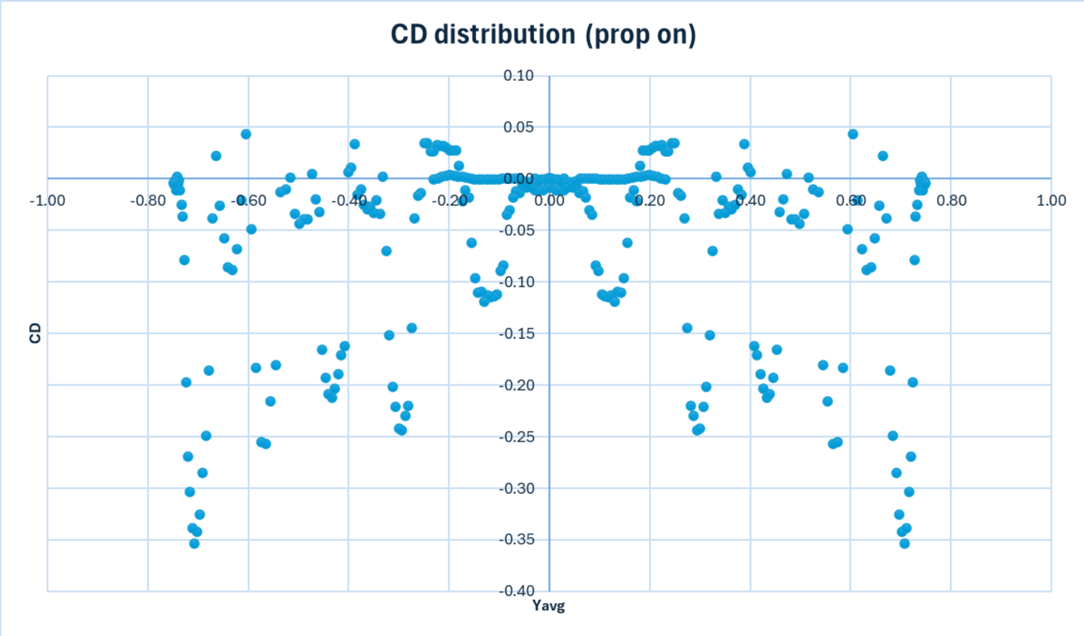

Figure 4.8: C_D distribution with propellers on at $\alpha = 4°$.

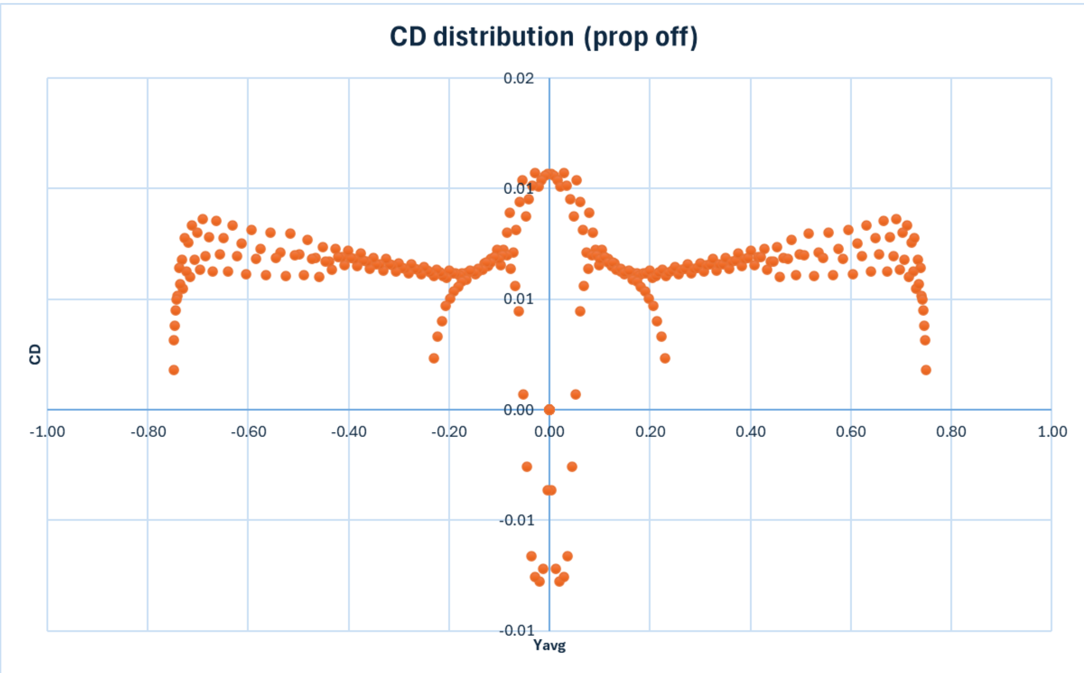

Figure 4.9: C_D distribution with propellers off at $\alpha = 4°$.

moving the propellers set 30 to 40 cm higher, so that the propellers did not blow right on the wing. Likewise previous analysis, in the induced polar, the CL curve has negative values, but this time

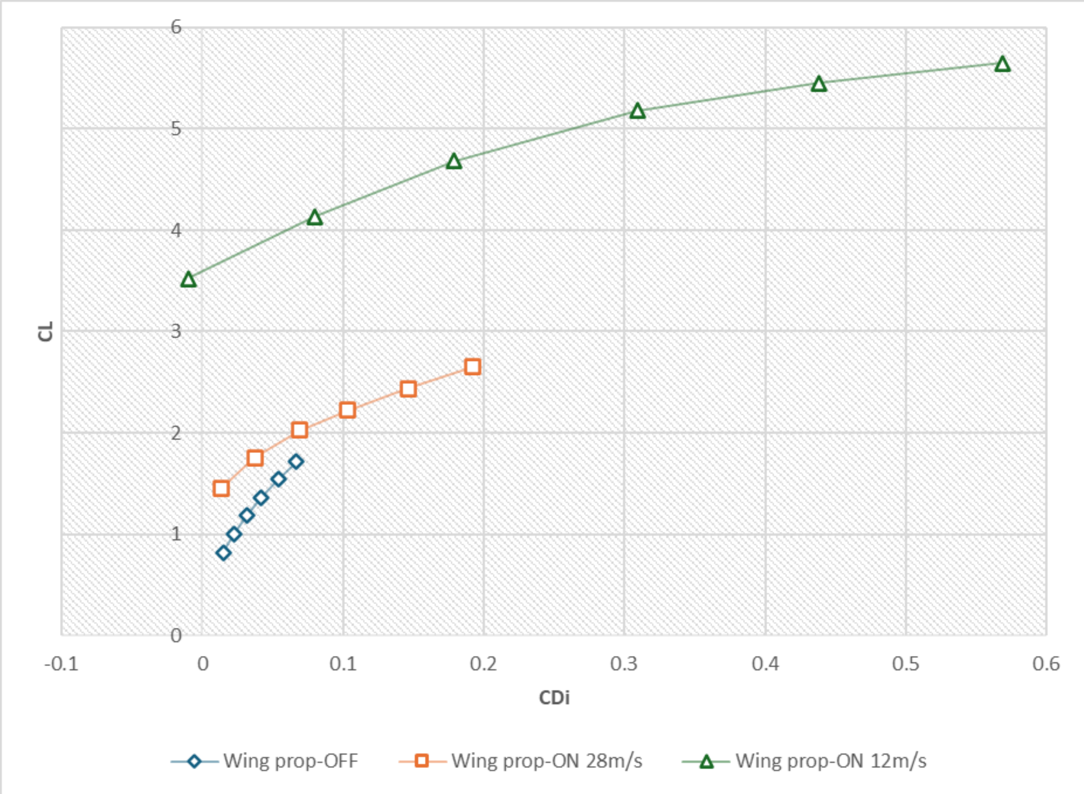

Figure 4.10: NASA X-57 C_L vs. C_{Di} polar.

shifted even further to the left than before as shown in Figure 4.11.

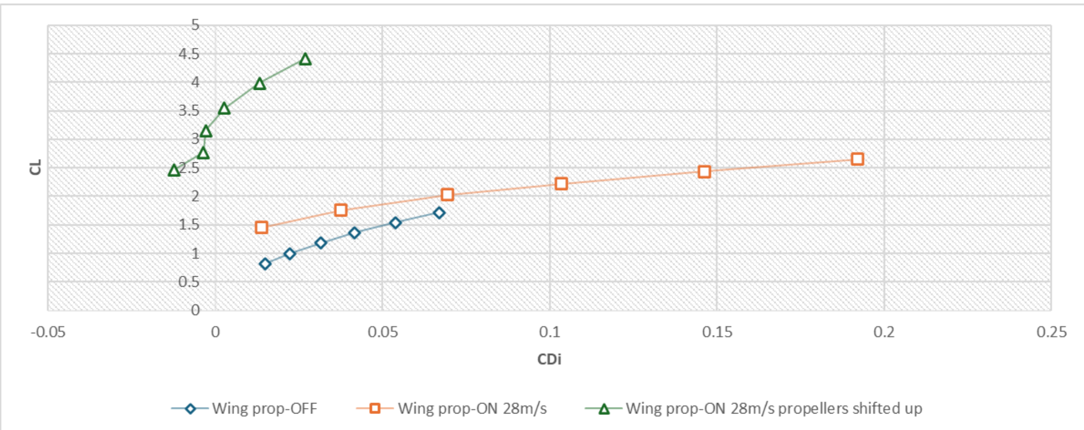

Figure 4.11: NASA X-57 C_L vs. C_{Di} polar with propellers shifted up.

Thus, the application of propellers to the VSPAERO VLM solver may provide unrealistic values of the drag coefficient, especially with low speed, high thrust conditions.

4.3 Effects of DEP with angle of sideslip

By changing settings on VSPAERO, this time setting up on *Flow Conditions*, as shown in Figure 4.12, six β points ranging from 0 to 10 deg, while only two α values, 0 and 4 deg, latero-directional results are evaluated.

Flow Condition					
Alpha Start	0.000	End	4.000	Npts	2
Beta Start	0.000	End	10.000	Npts	6
Mach Start	0.000	End	0.000	Npts	1
ReCref Start	400000	End	2e+07	Npts	1

Figure 4.12: Flow conditions with β variable.

Latero-directional analysis with propellers on and propellers off are pointed out with $\alpha = 0°$ in Figures 4.13 and 4.14 and with $\alpha = 4°$ in Figures 4.15 and 4.16. As expected, the latero-directional coefficients are insensitive to changes in angle of attack.

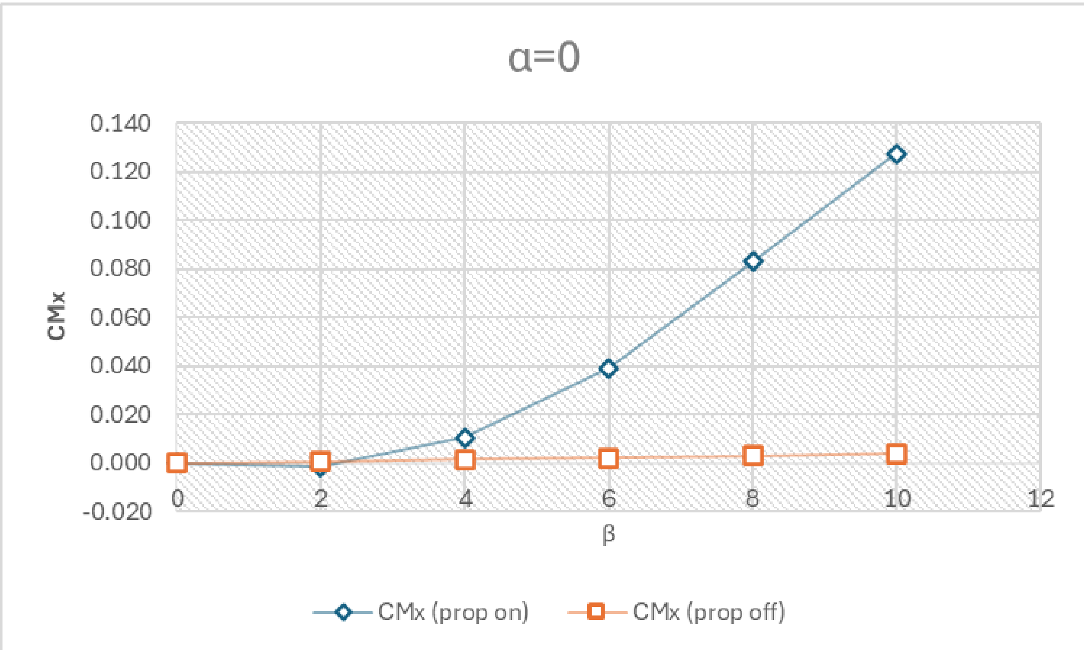

Figure 4.13: C_{Mx} vs. β comparison curves.

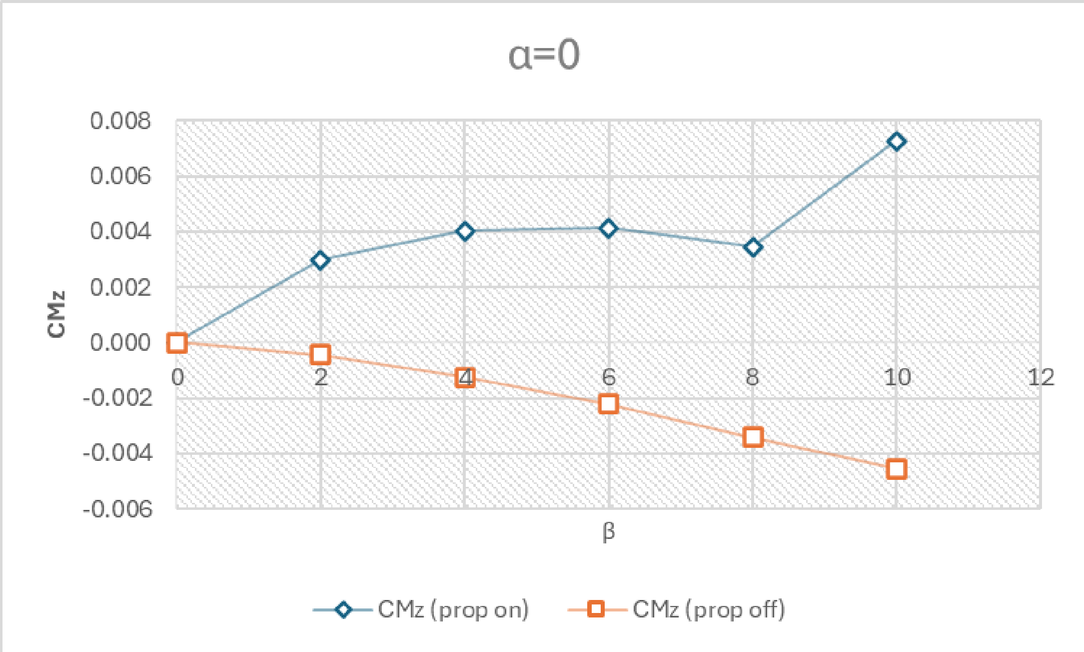

Figure 4.14: C_{Mz} vs. β comparison curves.

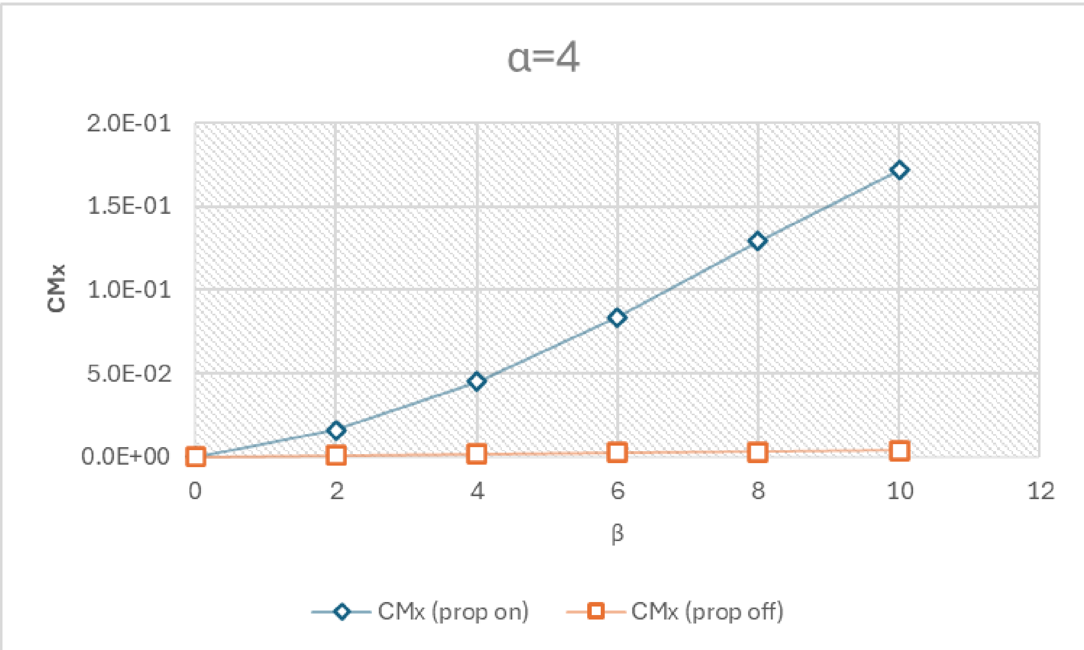

Figure 4.15: C_{Mx} vs. β comparison curves.

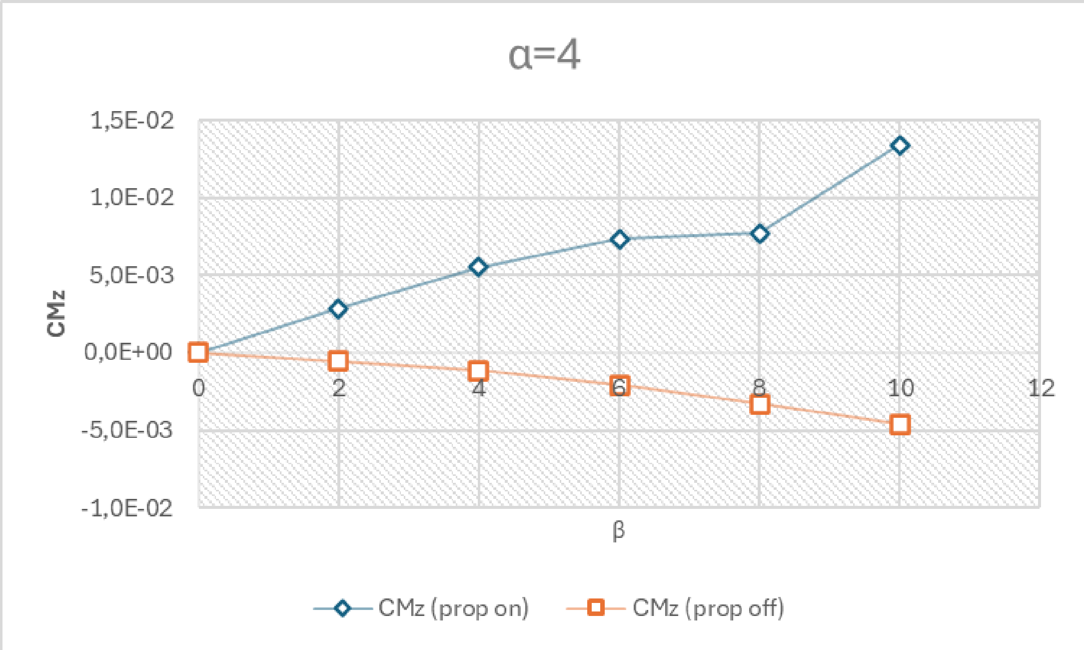

Figure 4.16: C_{Mz} vs. β comparison curves.

In Figures 4.17 and 4.18 C_{Mx} and C_{Mz} derivatives values comparison are shown.

	PROP ON	PROP OFF
$CM_{x\alpha}$	-8.883E-07	-7.97E-11
$CM_{z\alpha}$	5.087E-08	7.36E-09

Figure 4.17: $C_{Mx\alpha}$ and $C_{Mz\alpha}$ derivatives table.

	PROP ON		PROP OFF	
	α=0	α=4	α=0	α=4
$CM_{x\beta}$	0.1300	0.0180	0.0004	0.0004
$CM_{z\beta}$	0.0010	0.0010	-0.0005	-0.0005

Figure 4.18: $C_{Mx\beta}$ and $C_{Mz\beta}$ derivatives table.

4.4 Effects of DEP with flaps

The effect of flaps deflection at 15° and 30° is here discussed. First, in the *Control Surface Grouping* tab a grouped control surfaces was assigned to simultaneously select both flaps and the sign of the *Deflection Gain per Surface* of the left wing movable was changed to have the same rotation direction, as shown in Figure 4.19.

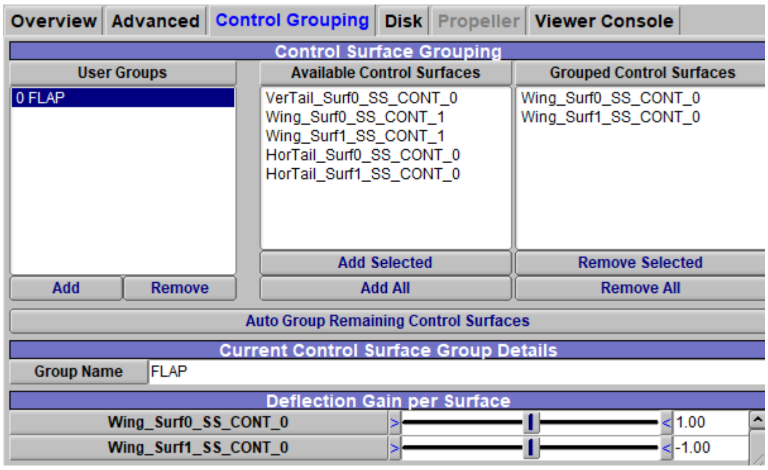

Figure 4.19: VSPAERO flap set up.

Then, the flap deflection value in deg is assigned in *Control Group Angles* in the *Overview* tab as in Figure 4.20.

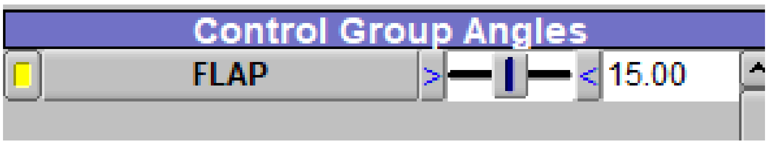

Figure 4.20: Flap angle set up.

Graphic results with and without propellers are shown in Figures 4.21 and 4.22 with flap deflection $\delta_f = 15°$.

While in Figures 4.23 and 4.24 it is possible to see comparison curves with and without propellers with flap deflection at 30°.

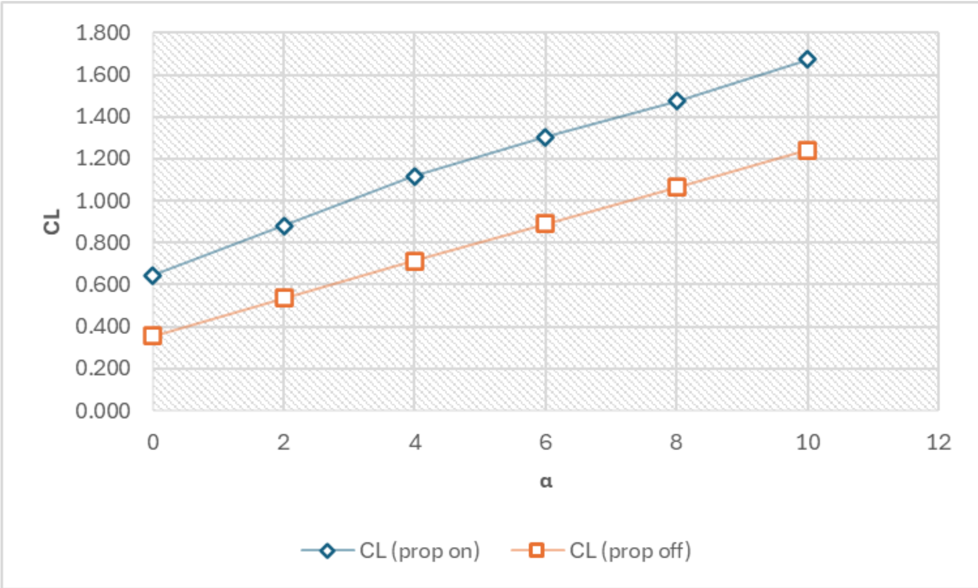

Figure 4.21: C_L vs. α comparison curves with flap deflection $\delta_\mathrm{f} = 15°$.

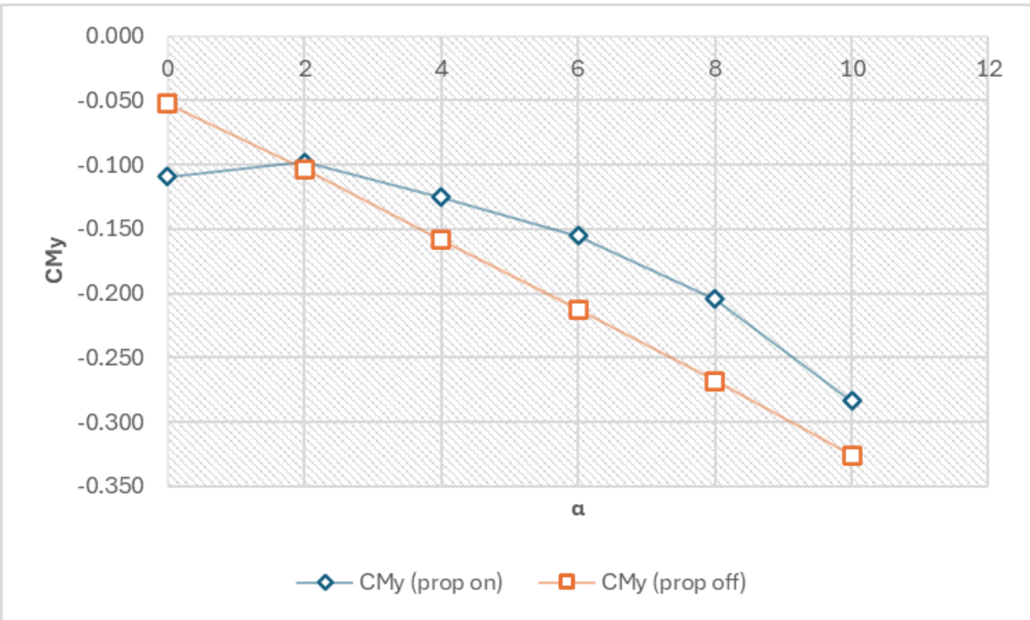

Figure 4.22: C_{My} vs. α comparison curves with flap deflection $\delta_\mathrm{f} = 15°$.

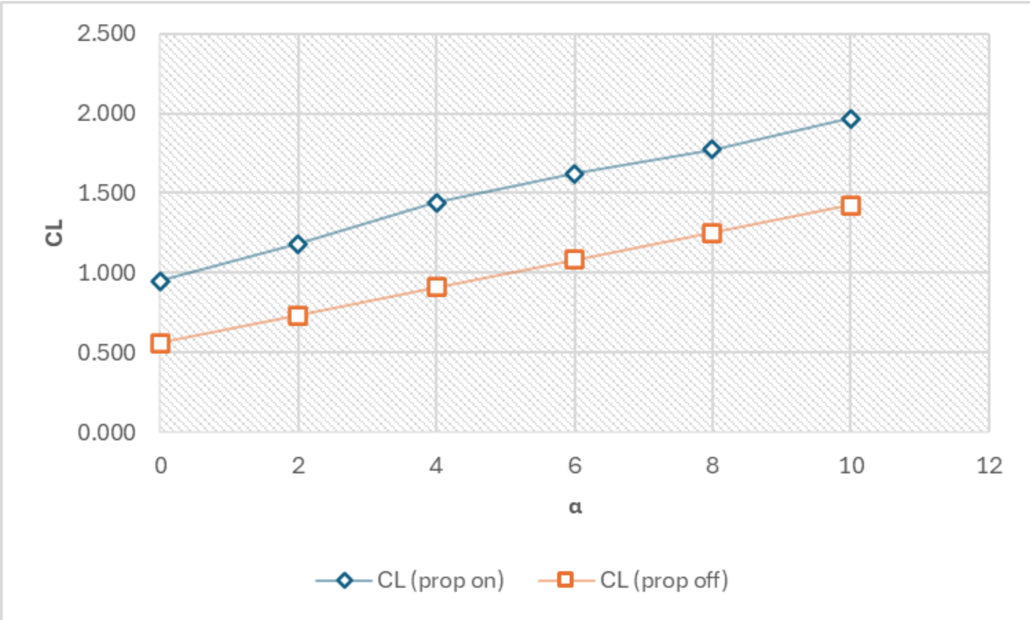

Figure 4.23: C_L vs. α comparison curves with flap deflection $\delta_{\mathrm{f}} = 30°$.

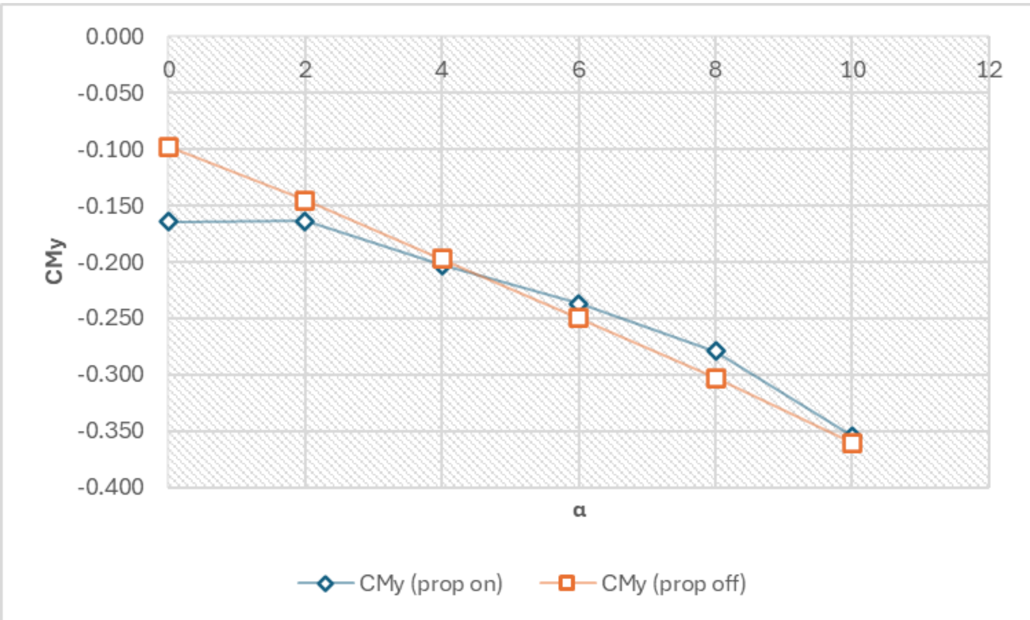

Figure 4.24: C_{My} vs. α comparison curves with flap deflection $\delta_{\mathrm{f}} = 30°$.

4.5 Effects of DEP with elevators deflection

Other analyses were done on three different flap deflection angles, and for each of them four elevator deflection angles: $10°$, $-10°$, $-20°$, and $-30°$. Analysis started with the setting of a new control grouping on VSPAERO (Figure 4.25) as seen previously with flaps.

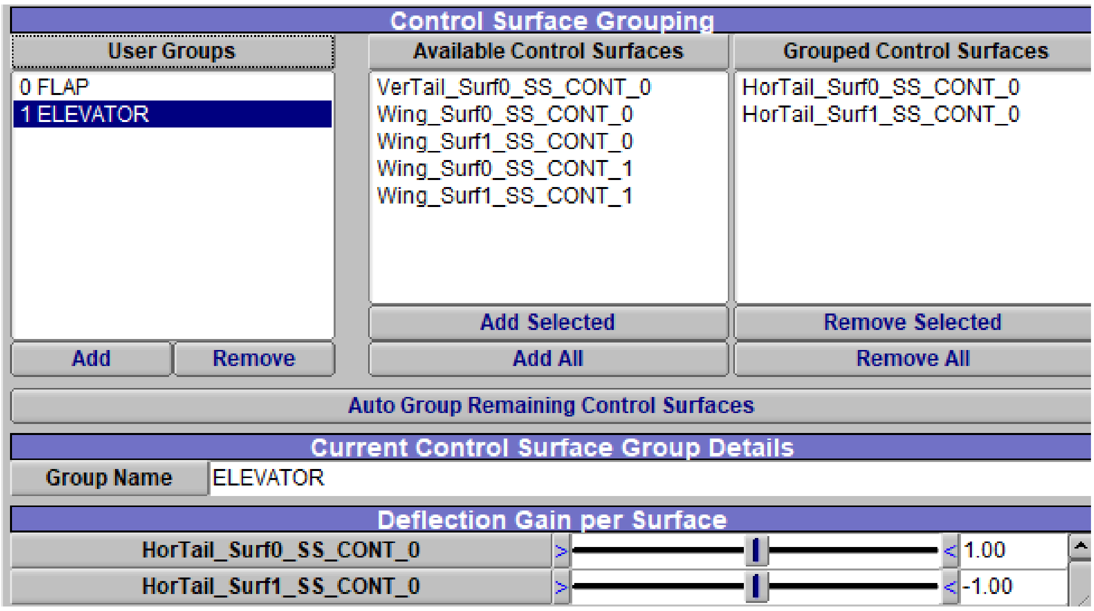

Figure 4.25: Creation of the elevator.

Then we settled up the required elevator deflection angle as in Figure 4.26.

Figure 4.26: Elevator angle deflection.

Lift coefficient curves with comparison between propellers on and propellers off are shown in Figures 4.27, 4.28, 4.29 and 4.30 first with $\delta_e = +10°$, then with $\delta_e = -10°$ and $\delta_e = -20°$ and lastly with $\delta_e = -30°$.

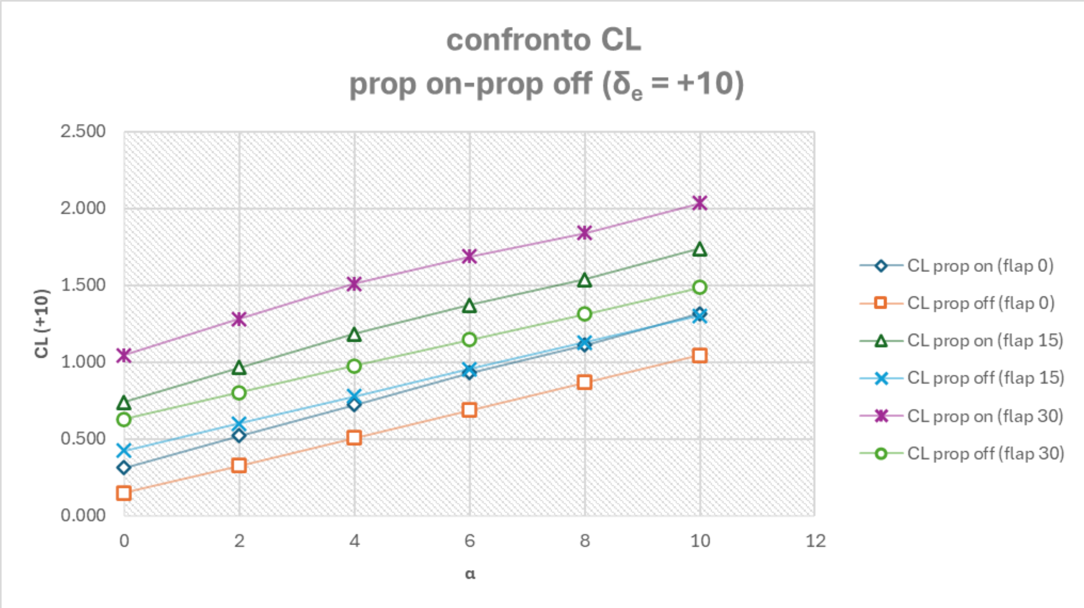

Figure 4.27: C_L vs. α comparison curves with $\delta_e = +10°$.

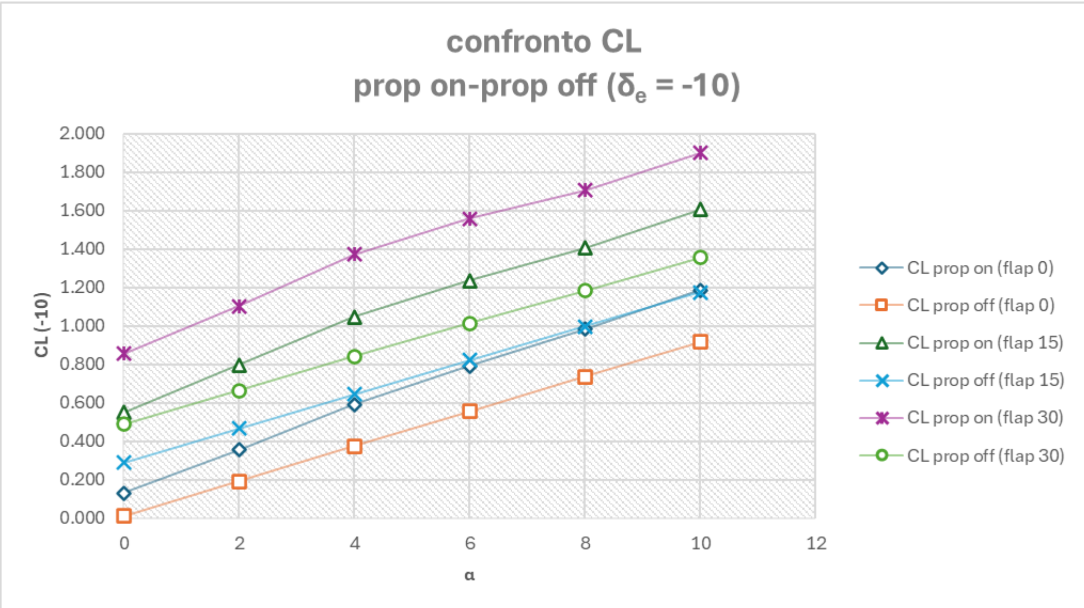

Figure 4.28: C_L vs. α comparison curves with $\delta_e = -10°$.

It is possible to notice that in the C_L plots, the propellers on curves at one flap configuration overlap another flap configuration with propellers off. According to VSPAERO solver results, the effect of distributed propulsion on the lift coefficient of this aircraft in clean configuration is equivalent to the propellers off configuration

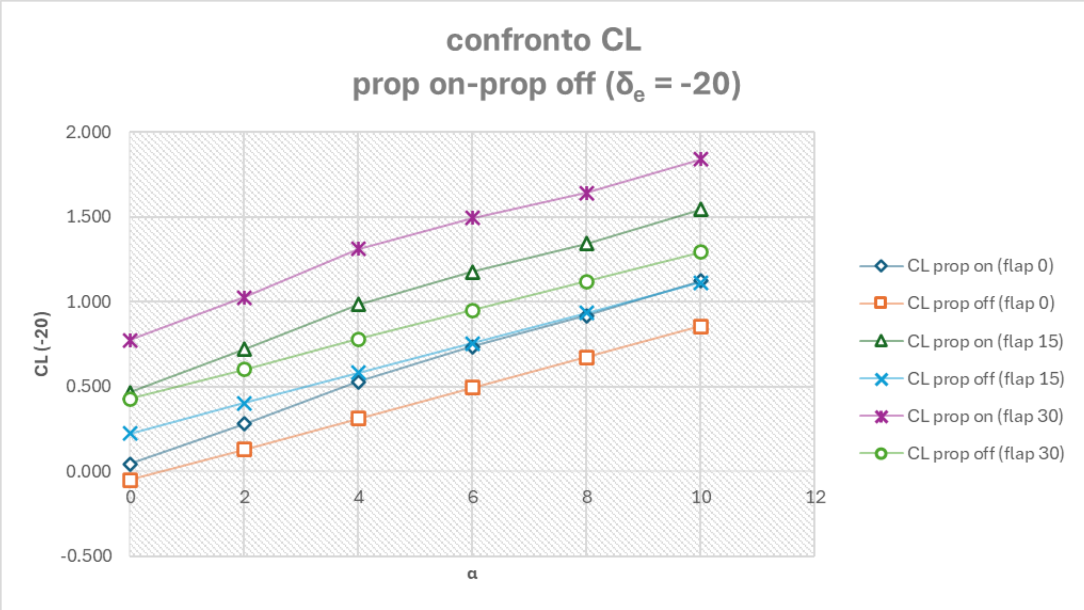

Figure 4.29: C_L vs. α comparison curves with $\delta_e = -20°$.

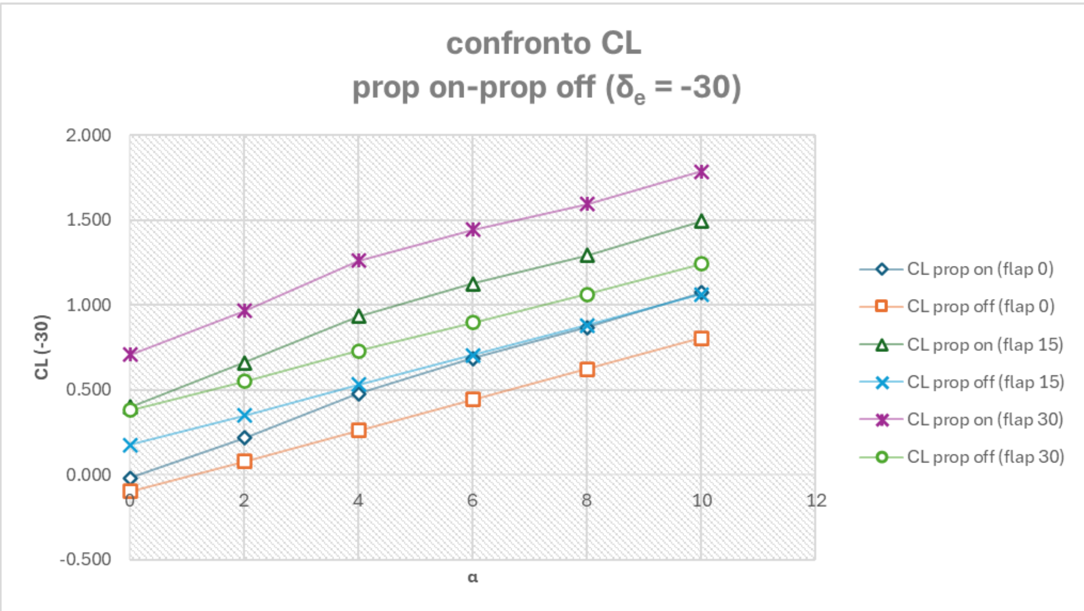

Figure 4.30: C_L vs. α comparison curves with $\delta_e = -30°$.

with flap deflection angle of 15°.

Lastly we have C_{My} comparison curves in Figures 4.31, 4.32, 4.33 and 4.34.

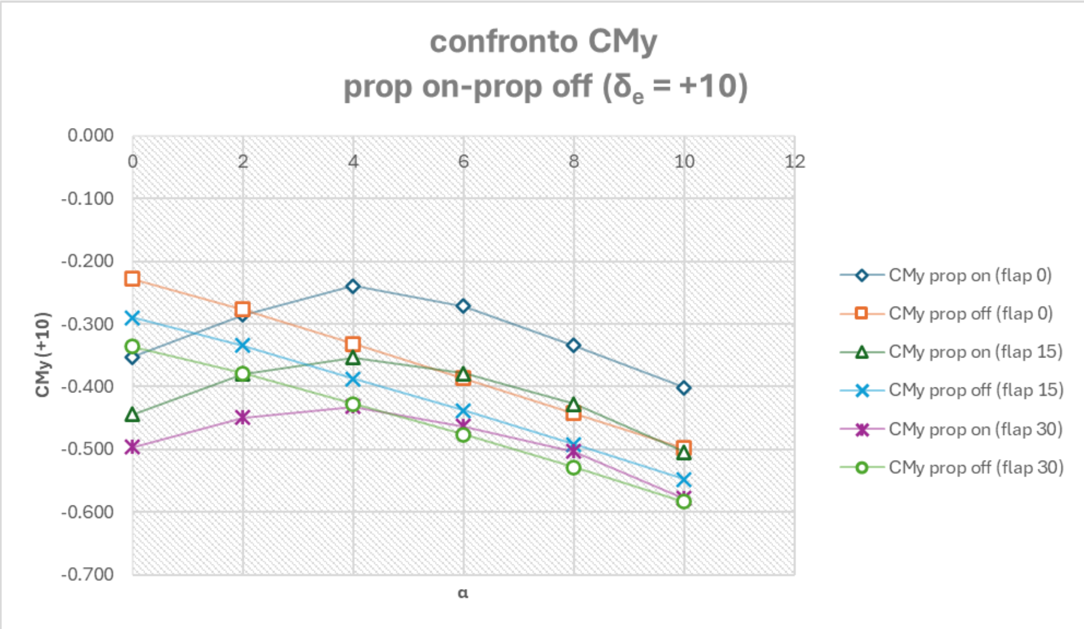

Figure 4.31: C_L vs. α comparison curves with $\delta_e = +10°$.

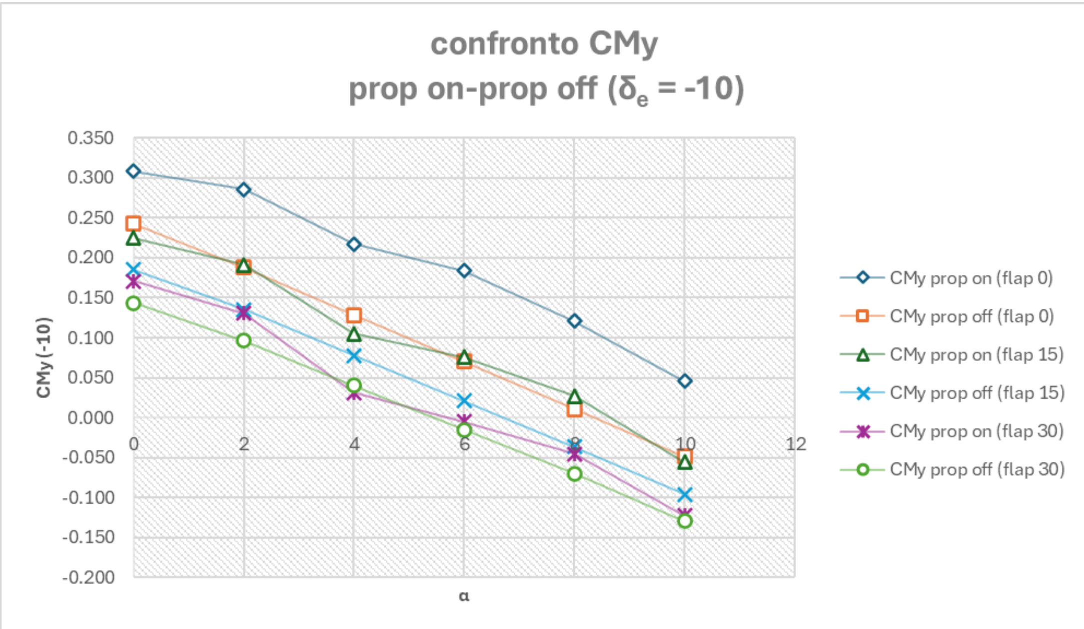

Figure 4.32: C_{My} vs. α comparison curves with $\delta_e = -10°$.

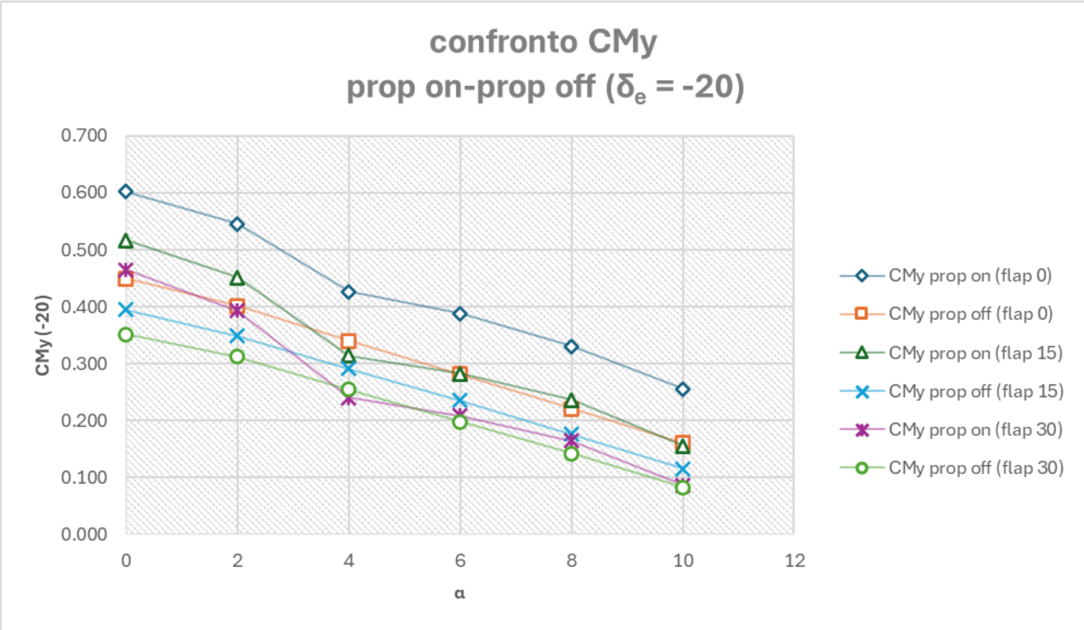

Figure 4.33: C_{My} vs. α comparison curves with $\delta_e = -20°$.

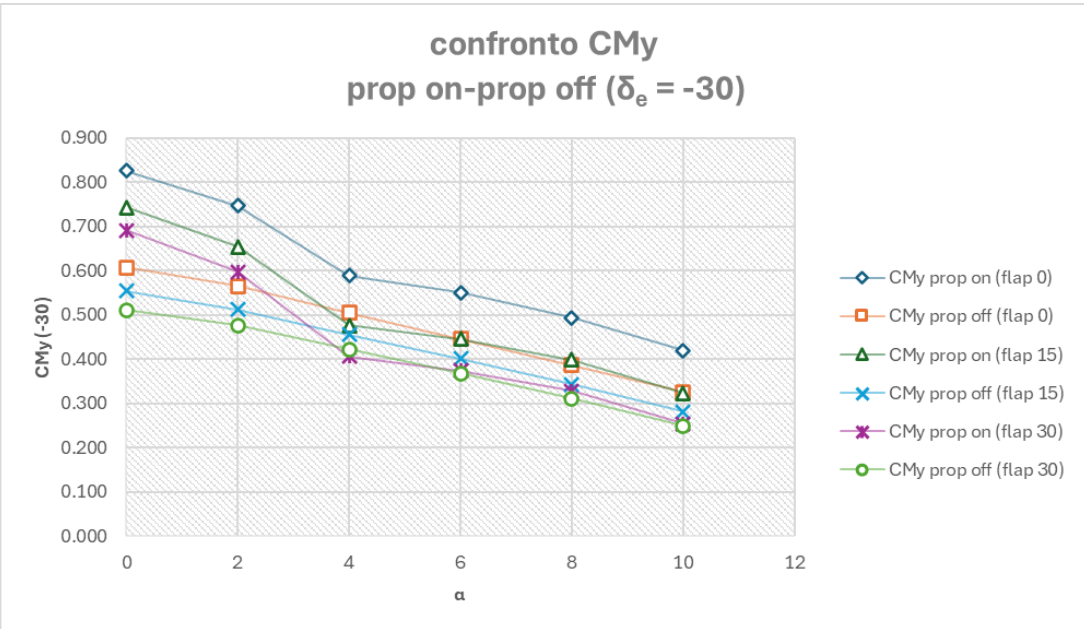

Figure 4.34: C_{My} vs. α comparison curves with $\delta_e = -30°$.

Chapter 5

Stability and Control Consideration

5.1 Aerodynamic derivatives

Through the Microsoft Excel function `SLOPE` it was possible to evaluate the stability derivatives: $C_{L\alpha}$, $C_{M\alpha}$, C_{L0}, and C_{M0}, comparing propellers on (Figure 5.1) and propellers off results (Figure 5.2), at different flap δ_{f} and elevator δ_{e} angles deflection.

	δe=0			δ_f=0			
	δ_f=0	δ_f=15	δ_f=30	δe=+10	δe=-10	δe=-20	δe=-30
CL_α	0.103	0.101	0.101	0.100	0.105	0.107	0.109
CM_α	-0.018	-0.017	-0.019	-0.006	-0.026	-0.035	-0.040
CL_0	0.225	0.645	0.951	0.311	0.130	0.045	-0.020
CM_0	-0.013	-0.110	-0.164	-0.353	0.308	0.602	0.827

	δ_f=15				δ_f=30			
	δe=+10	δe=-10	δe=-20	δe=-30	δe=+10	δe=-10	δe=-20	δe=-30
CL_α	0.099	0.104	0.106	0.108	0.097	0.103	0.105	0.107
CM_α	-0.007	-0.027	-0.035	-0.041	-0.009	-0.029	-0.037	-0.043
CL_0	0.740	0.550	0.466	0.401	1.046	0.854	0.774	0.707
CM_0	-0.444	0.225	0.517	0.744	-0.496	0.171	0.465	0.692

Figure 5.1: Stability derivatives with propellers on.

It is possible to note that in many cases aerodynamic derivatives are a fair approximation of the curve points trend, while there are some values of $C_{M\alpha}$ close to zero, due to the curve slope that first

	$\delta e=0$			$\delta_f=0$			
	$\delta_f=0$	$\delta_f=15$	$\delta_f=30$	$\delta e=+10$	$\delta e=-10$	$\delta e=-20$	$\delta e=-30$
CL_α	0.094	0.088	0.086	0.090	0.091	0.091	0.090
CM_α	-0.025	-0.027	-0.026	-0.027	-0.029	-0.029	-0.029
CL_0	0.089	0.356	0.560	0.148	0.011	-0.051	-0.098
CM_0	-0.008	-0.053	-0.098	-0.229	0.243	0.450	0.608

	$\delta_f=15$				$\delta_f=30$			
	$\delta e=+10$	$\delta e=-10$	$\delta e=-20$	$\delta e=-30$	$\delta e=+10$	$\delta e=-10$	$\delta e=-20$	$\delta e=-30$
CL_α	0.088	0.089	0.089	0.089	0.086	0.086	0.086	0.086
CM_α	-0.026	-0.028	-0.028	-0.027	-0.025	-0.027	-0.027	-0.027
CL_0	0.425	0.287	0.225	0.177	0.629	0.489	0.427	0.380
CM_0	-0.290	0.185	0.395	0.554	-0.336	0.143	0.351	0.511

Figure 5.2: Stability derivatives with propellers off.

rises and then falls, as shown in Figure 4.31.

Eventually, two more tables were generated: the first one (Figure 5.3) with the differences between propellers on and propellers off aerodynamic derivatives values, and the latter (Figure 5.4) with propellers on and propellers off aerodynamic derivatives ratio in absolute value. These calculation are again evaluated with different flap and elevator angle of deflection.

	$\delta e=0$			$\delta_f=0$			
	$\delta_f=0$	$\delta_f=15$	$\delta_f=30$	$\delta e=+10$	$\delta e=-10$	$\delta e=-20$	$\delta e=-30$
CL_α	0.009	0.013	0.014	0.010	0.015	0.017	0.019
CM_α	0.007	0.010	0.007	0.021	0.003	-0.005	-0.012
CL_0	0.136	0.289	0.391	0.163	0.119	0.096	0.079
CM_0	-0.005	-0.057	-0.067	-0.124	0.065	0.153	0.219

	$\delta_f=15$				$\delta_f=30$			
	$\delta e=+10$	$\delta e=-10$	$\delta e=-20$	$\delta e=-30$	$\delta e=+10$	$\delta e=-10$	$\delta e=-20$	$\delta e=-30$
CL_α	0.011	0.015	0.018	0.019	0.012	0.017	0.019	0.021
CM_α	0.019	0.001	-0.007	-0.014	0.016	-0.002	-0.010	-0.017
CL_0	0.315	0.263	0.242	0.224	0.417	0.365	0.347	0.327
CM_0	-0.154	0.040	0.122	0.190	-0.160	0.027	0.113	0.180

Figure 5.3: Difference between the values of Figure 5.1 (propellers on) and Figure 5.2 (propellers off).

	δe=0			δ_f=0			
	δ_f=0	δ_f=15	δ_f=30	δe=+10	δe=-10	δe=-20	δe=-30
CL_α	1.10	1.15	1.17	1.11	1.16	1.19	1.20
CM_α	0.71	0.64	0.72	0.22	0.90	1.19	1.41
CL_0	2.53	1.81	1.70	2.10	11.80	-0.89	0.20
CM_0	1.58	2.08	1.68	1.54	1.27	1.34	1.36

	δ_f=15				δ_f=30			
	δe=+10	δe=-10	δe=-20	δe=-30	δe=+10	δe=-10	δe=-20	δe=-30
CL_α	1.13	1.17	1.20	1.22	1.14	1.19	1.21	1.24
CM_α	0.26	0.97	1.26	1.51	0.35	1.06	1.37	1.63
CL_0	1.74	1.92	2.08	2.27	1.66	1.75	1.81	1.86
CM_0	1.53	1.21	1.31	1.34	1.48	1.19	1.32	1.35

Figure 5.4: Ratio of the absolute values of Figure 5.1 (propellers on) and Figure 5.2 (propellers off).

Chapter 6

Conclusions

Drawing this thesis to a conclusion, it is clear to notice that VSPAERO turn out to be extremely beneficial for aircraft design. Particularly in early design stages, VSPAERO provides valid visions on the project aerodynamic characteristics. This approach simplify the design process, speeding it up and minimising the resource waste.

However is possible to come across some VSPAERO limitations, indeed as noticed in this thesis analysis, propellers simulation, under high thrust and low speed conditions, can lead to a completely erroneous drag values. Hence results do not truly reflect the actual values because flow conditions are simplified in line with its primary function of providing rapid, even if approximate, outcomes. Therefore it is necessary to verify analysis with higher fidelity method to make them as accurate as possible.

Furthermore an accurate aircraft design development influences the relevance of results obtained through VSPAERO. Despite of its limitations on complex models project, VSPAERO is a valid tools to evaluate initial numerical analysis for simple aircraft designs, before testing them in wind tunnel.

Ultimately, VSPAERO is a crucial software for models that require a rapid preliminary aerodynamic analysis under specific initial conditions, as it was possible to examine in this thesis.

Bibliography

[1] Nicholas K Borer et al. "Design and performance of the NASA SCEPTOR distributed electric propulsion flight demonstrator". In: *16th AIAA Aviation Technology, Integration, and Operations Conference*. 2016, p. 3920.

[2] Hyun D Kim, Aaron T Perry, and Phillip J Ansell. "A review of distributed electric propulsion concepts for air vehicle technology". In: *2018 AIAA/IEEE Electric Aircraft Technologies Symposium (EATS)*. IEEE. 2018, pp. 1–21.

[3] Ambrosino - Di Martino. *Aerodynamic analysis and surrogate modelling of distributed propulsion on commuter and regional aircraft through VLM and CFD methods*. 2018/2019.

[4] Joseba Murua, Rafael Palacios, and J Michael R Graham. "Applications of the unsteady vortex-lattice method in aircraft aeroelasticity and flight dynamics". In: *Progress in Aerospace Sciences* 55 (2012), pp. 46–72.

[5] Valentina Nasti. *Modelling of a 19-pax scaled airplane model and preliminary evaluation of its stability and control characteristics*. 2021/2022.

[6] OpenVsp. *OpenVsp*. Accessed 11 March 2024. URL: `https://hangar.openvsp.org/`.

[7] OpenVsp. *OpenVsp*. Accessed 18 March 2024. URL: `https://openvsp.org/learn.shtml`.